Tectonic control on the palaeogeographical evolution of the Miocene Seaway along the Western Alpine foreland basin

Amir Kalifi, Philippe Sorrel, Philippe Hervé Leloup, Albert Galy, Vincenzo Spina, Bastien Huet, Séverine Russo, Bernard Pittet, Jean-Loup Rubino

Accepted Manuscript

Geological Society, London, Special Publications

Tectonic control on the palaeogeographical evolution of the Miocene seaway along the Western Alpine foreland basin

Amir Kalifi, Philippe Sorrel, Philippe-Hervé Leloup, Albert Galy, Vincenzo Spina, Bastien Huet, Séverine Russo, Bernard Pittet & Jean-Loup Rubino

DOI: https://doi.org/10.1144/SP523-2021-78

To access the most recent version of this article, please click the DOI URL in the line above. When citing this article please include the above DOI.

Received 16 April 2021
Revised 7 December 2021
Accepted 10 December 2021

Tectonic control on the palaeogeographical evolution of the Miocene seaway along the Western Alpine foreland basin

Amir Kalifi[1,2], Philippe Sorrel[1], Philippe-Hervé Leloup[1], Albert Galy[3], Vincenzo Spina[2], Bastien Huet[2], Séverine Russo[2], Bernard Pittet[1], Jean-Loup Rubino[2,4]

[1] *Université de Lyon, UCBL, ENSL, CNRS, LGL-TPE, 69622 Villeurbanne, France*

[2] *Total SA, CSTJF, Avenue Larribeau, 64000 Pau, France*

[3] *CRPG, 15 rue Notre Dames des Pauvres, 54500 Vandœuvre-lès-Nancy, France*

[4]*ISTEP Campus P.& M. Curie, Sorbonne University, 4 place Jussieu, 75005, Paris*

ORCID ID: AK, 0000-0003-3041-1401; PS, 0000-0003-0074-5961; PHL, 0000-0001-6090-8772

Present address : AK, Total SA, CSTJF, Avenue Larribeau, 64000 Pau, France

*Corresponding author (e-mail: amir.kalifi@external.total.com)

Abstract: The Miocene of the Western Alpine foreland basin were deposited in a North-South seaway along the active alpine orogenic front. In the subalpine massifs and the southern Jura mountains, the revised Miocene stratigraphy documents a detailed chronology of thrust propagation at the western alpine front, where tectonic activity had a primary influence on seaway palaeogeographical evolution. Here we propose nine palaeogeographical maps during the Miocene, the first of which depicts the initial Miocene transgression at ~21.0 Ma. Between ~18.05 Ma and ~12.0 Ma, a westward retreat of the Miocene Sea occurred in response to the activation of the basal thrust of the Belledonne massif, which in turn triggered successive fault zones from east to west. At ~10.0 Ma, a major uplift phase intervened and induced a rapid southward retreat of the Miocene Sea. The reconstructed palaeogeographical maps outline the main controls on the foreland basin seaway evolution: (i) the timing of the main thrusts, (ii) the inherited palaeotopography and (iii) eustatic sea-level changes during the Miocene. These reconstructions are integrated at the basin scale, highlighting the southward to westward-directed seaway migration in response to the Belledonne thrust activity that deeply shaped the palaeogeographical evolution during the early to middle Miocene.

Keywords

Foreland basins, Seaway, Gilbert delta, Sequence stratigraphy, Tectonics, Miocene

Introduction

The last few decades have seen a growing interest in ancient straits and seaways successions related to their oil and gas reservoir potential. The constricted morphology of straits and seaways favours the amplification of marine currents (Defant 1961; Pugh 1987), as well as a complex interplay of processes (i.e., oceanic-, tidal-, bottom-, turbiditic- and wind-induced currents; Berné *et al.* 1988; Ferret 2011; Olariu *et al.* 2012; Reynaud and Dalrymple 2012; Reynaud *et al.* 2012, 2013; Longhitano *et al.* 2014; Rossi *et al.* 2017; De Weger *et al.* 2020). The formation of seaways is controlled by tectonic activity, which primarily impacts accumulation rates (Catuneanu 2004, 2019), whereas the palaeogeographical evolution of the seaway triggers the opening and closure of the sills as a result of

both tectonic activity and sedimentary input. In order to improve models constraining the evolution of depositional conditions and sedimentary dynamics of tectonically-influenced seaways, this study focuses on the Miocene seaway of the Western Alpine foreland basin. Located between the orogenic wedge and the adjacent craton (Dickinson 1974; DeCelles and Giles 1996), foreland basins often correspond to elongated and narrow basins that favour the development of seaways in front of and along the rising chain (hundred(s) of km in scale; Dickinson 1974; DeCelles and Giles 1996). In such geological settings, the palaeogeography constantly evolves under the influence of the migrating orogenic wedge towards the foreland basin; therefore, they represent ideal natural laboratories for studying the impacts of tectonics on the development (and the morphology) of straits and seaways.

The Western Alpine foreland basin results from the Alpine orogeny during the Cenozoic, and can be subdivided into three areas: (i) to the North, the North Alpine Foreland Basin (NAFB) borders the Central Alps between the Haute-Savoie region in France and Vienna in Austria, including the Swiss part of the basin also called the Swiss Molasse basin (SMB) (Fig. 1A); (ii) to the South, the Rhodano-Provencal Molasse Basin (RPMB) is located between the Devoluy massif, the Castellane arc, the Basse Provence area and the Valreas basin. Between these two main areas, (iii) the French subalpine massifs, the Southern Jura, the Bas-Dauphiné basin and the Bresse basin constitute a complex amalgamation of several geological domains. During the Miocene, alpine tectonic events involved a complex paleogeographical evolution of the Miocene seaway. In the NAFB, the Miocene chronostratigraphy, palaeogeography and deformation history is well constrained and suggest an upper Aquitanian/lower Burdigalian initial marine transgression preceding an upper Burdigalian-lower Langhian southward-directed sea retreat (Pfiffner 1986; Schlunegger *et al*. 1996; Kempf *et al.* 1997; Kempf and Matter 1999; Strunck and Matter 2002; Berger *et al.* 2005; Kalin *et al.* 2009; Grunert *et al.* 2012; Jost *et al.* 2016; Pipper and Reichenbacher 2017; Sant *et al.* 2017; Garefalakis and Schlunegger 2019; Hülscher *et al.* 2019). The origin of the lower Miocene transgression is, however, still debated (Strunck and Matter 2002; Berger *et al.* 2005). To the south, in the RPMB, a high-resolution Miocene chronostratigraphy allowed detailed paleogeographical reconstructions showing an upper Aquitanian/lower Burdigalian first marine transgression to the east and an upper Tortonian southward-directed sea retreat (Rubino *et al.* 1990; Besson *et al.* 2005). In the literature, different models of the Miocene palaeogeographical evolution at the Western Alpine foreland basin scale have been proposed (Rubino *et al.* 1990; Sissingh 2001; Ford and Lickorish 2004). However, the lack of timing control in the hinge area between the SMB and the RPMB (the French subalpine massifs, the Southern Jura and adjacent basins) hinders the reconstruction of Miocene palaeogeography at high-temporal resolution, which directly hampers our understanding of the impact of tectonic activity on the Miocene seaway evolution (e.g., marine connexions, basins configuration).

This paper aims at filling this gap by reappraising the impact of tectonic activity on the Miocene seaway palaeogeographical evolution of the Western Alpine foreland basin in focusing on the French subalpine massifs, southern Jura synclines and adjacent basins. For this purpose, a comprehensive palaeogeographical reconstruction of Miocene palaeoenvironments (over the course of the alpine deformation) is undertaken here, based on the synthesis of : (i) the Miocene depositional models as detailed in Kalifi *et al.* (2020) for the study area, (ii) a new eustatic-driven 3rd order sequence stratigraphy based on coupled biostratigraphical, magnetostratigraphical and chemostratigraphical dating applied on well-logs and sedimentological sections (Kalifi 2020, Kalifi *et al.* 2021) and (iii) an updated calendar of the alpine deformation relying on Kalifi *et al*. (2021). This complete dataset characterized by high-resolution timing controls is further used to highlight the tectonic control on the seaway paleogeographical evolution, including the evolution of marine connexions and marine

conditions, the localization of the main fluvial inputs (entry points), the impact of basin configuration and their evolution during the Miocene.

Eventually, this study tackles long-lasting palaeogeographic issues between the Swiss Molasse Basin to the north and the Rhodano-Provencal Molasse basin to the south. Palaeogeographical reconstructions are finally compared at the scale of the Western Alpine foreland basin in order to highlight the impact of active tectonics on the Miocene seaway palaeogeographical evolution.

Geological setting

This study focuses on the Miocene succession of the Western Alpine foreland basin, which corresponds to the peripheral foreland basin of the Cenozoic Alpine orogeny (Fig. 1A). It includes (i) the French subalpine massifs (i.e., the Vercors, the Chartreuse and the Bauges massifs) and the southern Jura (Fig. 1B). In these areas, the Miocene deposits constitute the infill of piggy-back basins; (ii) the Bas-Dauphiné, the La Bresse and the Crest adjacent basins (Fig. 1B), where Miocene deposits represent the infill of the foreland basin and are poorly deformed. The study area is bordered to the east by the Belledonne massif (Fig. 1B, C), which is part of the External Crystalline Massifs, and to the west by the adjacent craton corresponding to the Massif Central (Fig. 1B).

In the study area, the Miocene deposits derive from the second shallowing-upward cycle of the Western Alpine foreland basin overfilled phase (Mid-Oligocene to the Late Miocene; Sinclair and Allen, 1992; Ford and Lickorish, 2004; Ford *et al.* 2006). Before the first Miocene marine transgression (i.e., during the Oligocene and the lower Aquitanian), an extensional phase related to the "Oligocene Western European Rift" (OWER) occurred (Debelmas 1974; Curial 1986; Bergerat 1987; Ziegler 1988, 1990, 1994; Bergerat *et al.* 1990) whereas, to the east, the study area was already affected by the Alpine compression (Doudoux *et al.* 1982). Hence a complex palaeotopography was inherited from the Oligocene, as discussed later in this study. The Miocene succession was therefore deposited in a North-South narrow and shallow corridor along the active alpine orogenic front that connected the Paratethys in the north (actual Swiss Molasse basin) to the Mediterranean Sea (ex-Tethys) in the south (Demarcq 1970; Bass 1991; Allen and Bass 1993; Fig. 1A).

The Miocene stratigraphy of the study area is characterized by 11 eustatically-driven sedimentary sequences over the entire zone, between the upper Aquitanian (~21.0 Ma) and the Tortonian (~8.2 Ma; Fig. 2A, B). These sequences were dated with a precision of ~0.5 Ma by using $^{87}Sr/^{86}Sr$ ages combined with biostratigraphical and magnetostratigraphical data (Kalifi 2020; Kalifi *et al.* 2021). The study area has been subdivided into 12 palaeogeographical zones (A to I, Figs. 1B and 2C), which were grouped into four palaeogeographical domains (based on a similar chronostratigraphy) (Fig. 2C). From east to west:

(1) the « oriental domain » includes zone A (Rumilly-Chambéry synclines) and zone B (Lans-Proveyzieux synclines) (Figs. 1B and 2C). In this domain, the first Miocene marine transgression took place with the deposition of the S1a sequence and is dated to the late Aquitanian (~21.0 Ma). The youngest Miocene deposits that crop out today in this domain correspond to upper Burdigalian to lower Langhian sequences (S2a, S2b, S3);

(2) the « median domain » includes zone C (Novalaise syncline), zone D (Voreppe syncline), and zone E (Rencurel-Méaudre synclines) (Figs. 1B and 2C). In this domain, the first Miocene marine transgression took place during the upper Burdigalian, coevally with the deposition of sequence S2a (~17.8 Ma); conversely, the latest deposits are Serravallian in age (sequence S5, and possibly S6);

(3) the « occidental domain » includes several zones in the Bas-Dauphiné basin: zone F (Bièvres region), zone G (Royans syncline), zone H (La Tour-du-Pin area), zone J (Bonnevaux plateau), zone K (Chambaran plateau) and zone L (Crest basin) (Figs. 1B and 2C). In this domain, the first Miocene marine transgression occurred during the deposition of S2a or S3. Upper Aquitanian and lower Burdigalian sequences (S1a and S1b) are absent, and upper Burdigalian sequences (S2a and S2b) are very discontinuous spatially (even sometimes absent). All the depositional sequences between the S3 (starting at ~16.2 Ma) and the topmost continental S8 (dated to ~8.2 Ma) were established by combining subsurface data (well-logs) and outcrops;

(4) the « La Bresse domain » only includes zone I (La Bresse basin) (Figs. 1B and 2C). The sedimentary infill is unique in this domain and consists of the upper Miocene marine sequences S6 and S7 (Serravallian – Tortonian; S6 [~12.0 to ~10.8 Ma] and the continental sequence S8 [~9.5 to ~8.2 Ma], Kalifi *et al.* 2021). Such a specific sedimentary infill is attributed to the inherited SW-NE "Vienne-Chamagnieu" palaeo-high structure (Fig. 2C; Enay 1980; Gudefin *et al.* 1980; Demarcq *et al.* 1984) that isolated this part of the basin during the early to middle Miocene.

In the subalpine massifs and southern Jura, the primary tectonic structures correspond to cover folds and thrusts, striking NNE-SSW and rooted in the Belledonne basement thrust (Fig. 1B, C). These structures accommodate the last WNW-ESE shortening phase of the Alpine collision wedge (Doudoux *et al.* 1982; Menard and Thouvenot 1987; Mugnier *et al.* 1990; Bellahsen *et al.* 2014;). Restored sections of the sedimentary cover in the Vercors and Chartreuse massifs document that horizontal shortening increases from the south (6 km) to the north (22 km) (Mugnier *et al.* 1987; Philippe *et al.* 1996, 1998; Bellahsen *et al.* 2014). The thrusts that juxtapose Mesozoic units over Miocene units correspond to the SAL fault, the GF fault, and five successive thrust faults zones (FZ1 to FZ5 from east to west, Kalifi *et al.* 2021) resulting from the alpine compression, whose activity has been calibrated in time based on recently dated syntectonic deposits. Three major tectonic phases occurred between the middle Oligocene and the late Miocene (Fig. 2C, D). The phase P1 took place most probably between the upper Rupelian (~29 +/- 2 Ma) and the upper Burdigalian (18,05 +/- 0.25 Ma), and triggered the onset of the FZ1 activity, as suggested by thick tectonically-driven accumulations of Oligo-lower Miocene sediments at the footwall of FZ1 (Kalifi *et al.* 2021). The phase P2 was induced by the activation of the Belledonne thrust initiated during the upper Burdigalian (18.05 +/- 0.25 Ma) and lasted at least until the Serravallian (S5 sequence; ~14.0 to ~12.0 Ma). This tectonic phase involved the rapid advance of the thrust front from east to west, between the SAL fault, the GF fault, and FZ2, FZ3, FZ4 and FZ5. The phase P3 started during the Tortonian (~10 Ma) coevally to the deposition of S7 and S8 sequences and is characterized by the onset of the Jura front and a regional uplift (Kalifi *et al.* 2021).

Methods

For the elaboration of palaeogeographical maps (between the upper Aquitanian and the Tortonian), this study mostly relies on the Miocene chronostratigraphy and tectonostratigraphy presented in Kalifi *et al.* (2021). Dating control is based on $^{87}Sr/^{86}Sr$ ages obtained in the basal (transgressive) deposits of depositional sequences, which coincide with eustatic sea-level rises (Kalifi *et al.* 2020, 2021), highlighting that the depositional sequences are mainly eustatically-driven (except for S8). Note that error bars for $^{87}Sr/^{86}Sr$ ages obtained within different palaeogeographical zones do not allow the identification of diachronous transgressions. Therefore, we assume that each transgression occurred sub-synchronously at the scale of the study area, and the age of the eustatic sea-level rise (for each

period) is used as the age of the transgression and of the depositional sequence at the basin scale. Depositional sequences were identified based on the evolution of facies associations and the main stratigraphical surfaces (Embry 1993, 1995), as detailed in Kalifi *et al.* (2020, 2021). Depositional sequences were further cross-checked using Posamentier and Allen (1999)'s methodology on spontaneous potential and gamma-ray logs data from 28 well-logs located in the Bas-Dauphiné basin (Kalifi 2020; Kalifi *et al.*, 2021). The maximum flooding deposits of the depositional sequences allowed the definition of nine palaeogeographic maps, at the regional scale. The palaeogeographical environments were interpreted based on the facies model presented in Kalifi *et al.* (2020). In the subalpine massifs and southern Jura area, which were affected by shortening during the Miocene, the initial width of the seaway was estimated by using the horizontal shortening values proposed by Philippe *et al.* (1996, 1998) and Bellahsen *et al.* (2014).

The large-scale geometries and the inherent spatial distribution of sedimentary facies in the stacked Gilbert deltas of the steep Pont-Demay cliffs were studied by deploying a drone (DJI Phantom 4 advanced). Based on overlapping georeferenced aerial photographs, a 3D model was built using the Agisoft software, and was then interpreted using the VRGS (Virtual Reality Geological Studio) digital outcrop modelling software.

Five strontium (Sr) isotope dating (i.e., chemostratigraphy) was newly performed in the Valréas basin in order to better constrain the lower Miocene palaeogeographical reconstructions at the scale of the western alpine foreland basin. Sr isotope ratios were measured on marine carbonate skeletons (oysters and pectens) at the CRPG (Centre de Recherches Pétrographiques et Géochimiques) in Nancy, France. A thorough inspection of shells was preliminarily conducted using stable isotope ratios ($\delta^{13}C$ and $\delta^{18}O$) to evaluate possible diagenetic disturbance (Hudson 1975, 1977; Nelson and Smith 1996). Corresponding ages are derived from measured $^{87}Sr/^{86}Sr$ ratio using the LOWESS non-parametric regression curve of McArthur *et al.* (2012); see Kalifi *et al.* (2020, 2021) for more details.

Results and Interpretations

In this section, the Miocene palaeogeographical evolution of the study area is reconstructed for sedimentary sequences S1 to S8, as dated in Kalifi *et al.* (2021). The palaeolandscape invaded during the marine transgression is likely to influence the morphology of the seaway, which in turn directly impacts the hydrodynamic processes acting during the deposition of sediments (Belknap and Kraft 1985; Malikides *et al.* 1988; Frouin *et al.* 2007; Longhitano 2013). Therefore, it is crucial to constrain as much as possible the palaeotopography on which the initial Miocene marine transgression took place before undertaking detailed palaeogeographic maps of the Miocene seaway.

Palaeogeographic reconstructions of the study area

The Oligocene to lower Aquitanian – The inherited palaeotopography before the Miocene transgression

The Miocene deposits generally lie disconformably on the thick Mesozoic substratum, or conformably on Oligocene continental deposits (Gidon *et al* 1978; Bass 1991; Butler 1992; Allen and Bass 1993; Kalifi *et al* 2020). An isopach map of Oligocene deposits highlighting the location of ante-Miocene palaeo-highs (Fig. 3) was constructed based on well-logs data (from the BRGM, "Bureau de recherches géologiques et minières"), seismic profiles (Kalifi *et al.* 2021) and surface data from geological maps (BRGM). In our study area, Oligocene sedimentary deposits are characterized by clayey-marly sediments intertwined with lacustrine limestones (Latreille 1969). The boundary between the eastern border of the Massif Central and the Bas-Dauphiné basin corresponds to a half-

graben characterized by an eastward-dipping normal fault, as suggested by profile 82SE01 (Mascle *et al.* 1996; Kalifi *et al.* 2021), with Oligocene strata thickening and diverging towards the fault (Fig. 3). Along the western border of the Bas-Dauphiné basin, GVA-1 well-log data indicate 1755 m of Oligocene deposits in the hangingwall of the Massic Central normal fault (Fig. 3). In turn, the CL-1 well reports Eocene deposits resting directly upon the basement, and subsequently overlain by 923m of Oligocene sediments. This suggests that the normal fault was active during the Oligocene and involved the initiation of a depocenter that developed sub-parallel to the normal fault (Fig. 3). This tectonic activity is consistent with the Oligocene extensional phase related to the "Oligocene Western European Rift" (OWER) as described at the European scale (Debelmas 1974; Hirn 1980; Curial 1986; Bergerat 1987; Ziegler 1988, 1990, 1994; Bergerat *et al.* 1990; Sissingh 2003; Prodehl and Haak 2006).

On the eastern border of the Bas-Dauphiné basin, another Oligocene depocenter extends between the Isère valley to the north, and the Royans syncline to the south (Fig. 3). The 91VER-1 profile highlights an inverted eastward-dipping normal fault (Kalifi *et al.* 2021) located eastwards from the BR-1 and BRF-1 wells. To the east of this fault, thin Oligocene deposits were recorded (VAF-1 and VAF-2 wells). In contrast, to the west of this fault, the absence of Oligocene deposits in the BR-1, BRF-1, CHF-1, BI-1, BIF-1, PA-1 wells suggests the presence of a topographical high already present during the Oligocene, which corresponds to the Montmiral-high (ML Palaeohigh, Fig. 3). Thus, during the Oligocene, the ML Palaeohigh was bordered to the east by a normal fault. This is consistent with the occurrence of coarse Oligocene deposits in the LTPF-1 well to the north (coarse pebbled sandstones) and the MO-3 wells in the south (reworked brecciated limestones), thus suggesting the proximity of a palaeorelief. To the north of the ML Palaeohigh, the Ile Cremieu also constituted a palaeo-high (IC Palaeohigh, Fig. 3). It was not flooded at least before the Serravallian, as suggested by karsts filled by siderolithic clays rich in mammal remains (see points H10 to H13 on Fig. 1B) dated between the Burdigalian and the Serravallian (Guérin and Mein 1971; Maridet *et al.* 2000; Maridet 2002, 2003; Mein and Ginsburg 2002; Costeur 2005).

Along the western border of the Royans syncline (Fig. 3), the Oligocene infill is controlled by eastward-dipping normal faults visible on the 82SE01 profile (Kalifi *et al.* 2021), as exhibited by a net decrease in the thickness of Oligocene deposits to the west (Fig. 3). This implies that the western border of the Royans syncline (Monts-du-Matin mountain) was most likely a palaeo-high (MM Palaeohigh, Fig. 3) during the Oligocene, but not much earlier than the Oligocene. This hypothesis is supported by the presence of kaolinite (originating from the alteration of the Massif Central granites (Dasarthi 1965) in the fluvial Eocene sedimentation of the Royans syncline, which involves the absence of the MM Palaeohigh during the Eocene. During the Miocene subalpine compression (Fig. 2), the Royans area was folded into a syncline at the footwall of FZ3 (Fig. 1B), which then corresponded to the western border of the Vercors massif (Kalifi *et al.* 2021). In the hangingwall of FZ3, the thickness of Oligocene sediments drastically decreases compared to the footwall of FZ3 and suggests, therefore, the highest topography to the east. Most probably, this topographic high likely resulted from the westward-dipping normal faults located on the hanging wall of FZ3 (Kalifi *et al.* 2021). Such a configuration implies that the Royans was most probably an ancient graben striking ~N-S (Fig. 3) likely formed during the Oligocene extensional phase (OWER). The Royans syncline was bordered by the MM Palaeohigh to the west, and the western border of the Vercors massif to the east, which also constituted a palaeohigh.

The evidence for a complex Oligocene palaeotopography not only concerns the Vercors massif, but also the western border of the sub-alpine massifs (Vercors, Chartreuse) and the eastern border of the southern Jura (Fig. 3), which are characterized by a total absence of Oligocene deposits. Furthermore,

the presence of East-West palaeovalleys on subcrop maps of the Miocene basal unconformity (Kalifi *et al.* 2020), as well as the occurrence of continental breccias on the western side of the Chartreuse massifs (Fig. 3), indicate that the entire western border of the sub-alpine massifs probably corresponded to a palaeohigh structure designed here as the Western Subalpine massif Palaeohigh (WSM Palaeohigh). The WSM Palaeohigh could then correspond to an ancient Oligocene horst, or even a rift shoulder.

To the east of the WSM Palaeohigh, between Chambéry and Annecy, Oligocene deposits are characterized by a gradual but rapid eastward-directed thickening-up trend (Fig. 3), as suggested from seismic profiles (88SV01, 88SV02-HR528, 88SV03). Along the WSM Palaeohigh, Oligocene sediments (i.e., alluvial fan deposits) are characterized by 0-20 m of clast-supported conglomerates showing eastward-directed palaeo-currents. To the east, Oligocene successions evolve to lacustrine or fine-grained alluvial-plain deposits, which progressively reach thicknesses > 1500m at the footwall of FZ1 (SV101, SV105, CHY1). This depocenter is most probably controlled by flexural subsidence at the footwall of the active FZ1 between 29 +/- 2 Ma and 18.05 +/- 0.25 Ma (Kalifi *et al.* 2021).

The upper Aquitanian to lower Burdigalian (S1a to S1b) – Tectonic loading induced by the FZ1

The upper Aquitanian to lower Burdigalian deposits characterize the advent of Miocene marine depositional environments and was only identified in the oriental domain (red points on Fig. 4) with two depositional sequences: S1a and S1b. Since marine deposits were confined between FZ1 to the east and the WSMPaleohigh to the west during the deposition of those two sequences, the basin is influenced by flexural tectonics induced by the activity of FZ1 (Fig. 2C, D).

The S1a sequence: 21.0 to 20.6 Ma. In the Rumilly-Chambéry synclines (zone A) of the oriental domain (Figs. 1B and 2C), the S1a transgression was dated at 21.28 +/- 0.32 Ma (Kalifi *et al.* 2021), which fits well with the T-2a eustatic transgression dated at ~21.0 Ma (Fig. 2B). The transgression occurred progressively at the top of the underlying lower Aquitanian continental deposits, which are interstratified with 1-5m thick marine sands (Bersier 1936, 1938; Bass 1991; Kalifi *et al.* 2021). This gradual transgression is consistent with the prevalence of a shallow marine environment during S1a, in line with the +10m sea-level rise characteristic of the T-2a eustatic transgression (Fig. 2B).

Along the western coast of the initial marine seaway, S1a starts with a 5 m (see points 1, 5b, 15 on Fig. 4) to 50 m thick (see point A6 on Fig. 4) bioclastic conglomeratic level. East- to north-east-directed palaeo-currents (see points 1, 5b, 15 on Fig. 4) highlight fluvial inputs from the WSM Palaeohigh, most probably through E-W incised valleys (Fig. 4, Kalifi *et al.* 2020). Except for this basal bioclastic conglomerate level along the western coast, the S1a is mainly represented by intertidal sandy deposits, which are locally interstratified with subtidal channels interpreted as being developed during the maximum flooding deposits (MF) of the S1a sequence (see point 1 on Fig. 4).

Further west, in the occidental domain (green points on Fig. 4), no S1a (and S1b) marine deposits were observed (Fig. 4). However, Latreille (1969) reported the presence of a specific unit covering the Bas-Dauphiné basin and stratigraphically located between the continental Oligocene deposits and the first Miocene marine deposits (upper Burdigalian, Kalifi *et al.* 2021), which could therefore correspond to the Aquitanian (S1a) or lower Burdigalian (S1b) deposits. This unit marks the sudden appearance of a petrographic composition of internal alpine origin (Latreille 1969) and the appearance of brackish molluscs and a lagoonal sedimentation in the Royans syncline (Giot 1943; see points 32, 34, 35 on Fig. 4). These two elements therefore suggest connexions with the seaway corresponding to S1a or S1b deposits to the east of the WSM Palaeohigh, in the oriental domain (Fig. 4). A marine

connexion with the Rhône valley to the south, through the Crest basin (Fig. 1B) is however excluded as no marine or lagoonal sediments during the S1a and S1b sequences were recorded in this basin (Depéret 1895; Demarcq *et al.* 1989; Kalifi *et al.* 2021).

The S1b (+S1c?) sequence: 20.6 to 17.8 Ma. The S1b transgression was dated at 20.4 +/- 0.35 Ma (Kalifi *et al.* 2021) in the Rumilly-Chambéry synclines of the oriental domain (zone A, Figs. 1B, 2C and 4), and matches with the T-2b eustatic transgression starting at ~20.6 Ma (Fig. 2B). The S1b is characterized by more distal marine deposits than S1a deposits, which is in accordance with the +25m sea-level rise of the T-2b (Fig. 2B). To the south, in zone B (Figs. 1B, 2C and 4), the S1b transgression was dated at 19.48 +/-0.63 Ma and coinciding well with the T-3a eustatic transgression (Fig. 2B). However, the absence of both S1a and the base of the S1b in zone B cannot be assessed as the basal Miocene deposits do not outcrop well there (5 to 10 m of observation gap).

Along the WSM Palaeohigh, in the north, S1b transgressive deposits are characterized by bioclastic conglomerates (see points 15, 5b on Fig. 4). A similar palaeogeographical configuration of eastward-directed fluvial inputs likely occurred in the WSM Palaeohigh, with alluvial fan deposits continuously accumulating over S1a and S1b. This is in line with the petrographic composition of clasts, initially dominated by upper Cretaceous sources but evolving upwards to the prevalence of lower Cretaceous limestones (Lamiraux 1977; see point A6 on Fig. 4). This evolution indicates a progressive erosion of the local relief (i.e., the WSM Palaeohigh), from younger to older sedimentary successions, which suggests a long-lasting exposure of the substratum (S1a and S1b). To the east, in a more distal position, distal marine deposits occurred with typical subtidal depositional environments (FA8 *sensu* Kalifi *et al.* 2020) characterized by tidal dunes showing palaeo-currents along a N-S seaway (see point 4 on Fig. 4). To the south, wave-dominated depositional environments are found (see points 7, 8, 10 on Fig. 4) indicating a generally mixed wave-tide transgression (Kalifi *et al.* 2020). The deepest environments are reached during the maximum flooding and correspond to open-coast subtidal depositional environments (FA6 *sensu* Kalifi *et al.* 2020). Sandstones are coarse-grained, glauconite-rich and contain rare exotic clasts (e.g., radiolarites, jaspers, granites) indicating a pervasive source from the exhumed internal Alpine areas to the east.

As described later in this study, a 3rd lower Burdigalian depositional sequence (S1c, ~19.0 to 17.8 Ma, Fig. 2A) was recognized in the Rhodano-Provencal molasse basin to the south (Fig. 1A). In the study area, poorly outcropping S1b (regressive) deposits prevent, however, accurate sequence stratigraphical interpretations, but do not exclude the presence of the S1c sequence.

The upper Burdigalian (S2a and S2b) – Onset of the Belledonne basal thrust

The upper Burdigalian deposits were observed and dated in the oriental domain (red points on Fig. 5), the median domain (blue points on Fig. 5) and in the eastern part of the occidental domain (zones F, G, K and L, Figs. 1 and 2C; green points on Fig. 5). These deposits are characterized by two depositional sequences: S2a and S2b.

The S2a sequence: 17.8 to 17.4 Ma. The S2a transgression occurred at 18.05 +/- 0.35 Ma, 17.95 +/- 0.2 Ma, 18.05 +/- 0.2 Ma, for zones A, C and E, respectively (Figs. 1B and 2C; Kalifi *et al.* 2021) and coincides with the T-4 eustatic transgression starting at ~17.8 Ma (Fig. 2B). S2a deposits also date the activation of the Belledonne basal thrust, which propagated to the surface through the SAL fault (Fig. 2D). The S2a depocenter was located near the longitude of the section n°4, where a ~740 m-thick succession (vs ~150 m at the section n°13 to the west) is found at the footwall of the SAL fault (Fig. 5A). A seismite of regional extension (zone A; Figs. 1B and 2C) reported within the transgressive

deposits of S2a, further supports a significant tectonic activity at that time (Kalifi *et al.* 2021). This may explain why the WSM Palaeohigh was flooded at that time, although the +30m sea-level rise of T-4 might have amplified the phenomenon (Fig. 2B).

Along the WSM Palaeohigh (~median domain; blue points, Fig. 5A), the onset of S2a is characterized by transgressive deposits (5-20 m thick) consisting of calcarenites rich in *Pecten Praescabriusculus*, bryozoans and corals. Transgressive deposits are overlain by thick silty-clay sediments typical of distal environments (offshore transition [FA2] to offshore [FA1] *sensu* Kalifi *et al.* 2020) corresponding to the S2a maximum flooding deposits. In the Vercors massif, these deposits are 1-2 m thick (see points 24, 25, E1, E2 on Fig. 5A), suggesting that the southern WSM Palaeohigh was topographically higher there. To the north-east of the WSM Palaeohigh, in the Rumilly-Chambéry synclines of the oriental domain (red points, Fig. 5A), transgressive deposits exhibit an additional unit between the basal *P. Praescabriusculus*-rich calcarenites and the S2a maximum flooding deposits, which is made of ~240 m-thick marine proximal deposits (open-coast intertidal [FA6] *sensu* Kalifi *et al.* 2020). Maximum flooding deposits consist of open-coast subtidal deposits with interstratified large-scale tidal dunes and open-coast intertidal deposits (respectively FA5, FA7, FA6 *sensu* Kalifi *et al.* 2020), suggesting that no definite offshore environments existed there at that time (sections n°4 and 5, Kalifi *et al.* 2020). The difference in S2a successions between the oriental and median domains likely resulted from the influence of the WSM Palaeohigh, on which less accommodation space was created. In the Isere valley, proximal sedimentation took place in zone B (see points B3, 9, 10 on Fig. 5A) with a conglomeratic unit that outlines the onset of the "Voreppe palaeo-delta" (*sensu* Bocquet 1966; Latreille 1969).

To the west of the WSM Palaeohigh and to the east of the IC Palaeohigh and ML Palaeohigh, in the Bas-Dauphiné basin (~occidental domain), the S2a maximum flooding deposits were identified in well-logs (VAF1, VAF2, MO2, SLF1, SL1; Fig. 5A). In this area, S2a sequence is characterized by clayey-marl deposits (~ the base of the regional unit called “St-Lattier" marls), therefore suggesting most probably distal depositional conditions. To the west of the IC Palaeohigh and ML Palaeohigh, no S2a (as well as the S2b) deposits were observed, implying that these palaeohighs corresponded to the western coast of the upper Burdigalian sea (Fig. 5). To the north of the Crest Basin, S2a disappears by onlapping directly on the north-western border of the MM Palaeohigh (Demarcq 1959; Jeannolin 1985). More to the north, the Royans syncline is also characterized by the absence of S2a. This suggests that, during S2a sequence, the MM Palaeohigh likely implied a bifurcation of the sea, and/or forced the sea to be confined between the MM Palaeohigh and the Massif Central (as proposed in Fig. 5A).

The S2b sequence: 17.4 to 16.2 Ma. The S2b transgression occurred at 17.20 +/- 0.15 Ma, 17.45 +/- 0.4 Ma, 17.28 +/- 0.47 Ma, 17.3 +/- 0.4 Ma, 17.48 +/- 0.23 Ma and 17.52 +/- 0.22 Ma for zones A, C, D, E, G, and L, respectively (Figs. 1B and 2C; Kalifi *et al.* 2021), that coincides well with T-5 eustatic transgression starting at ~17.4 Ma (Fig. 2B). S2b sequence records the ongoing propagation of the Belledonne basal thrust with the onset of the Gros Foug (GF) fault (Fig. 5B). In the hangingwall of the GF fault (Grésy-sur-Aix section, point 4 on Fig. 5B), an angular unconformity was observed at the top of S2a deposits and was dated at chron C5Dn (17.35 +/- 0.15 Ma, Kalifi *et al.* 2021). Subsequently, the S2b depocenter was recorded at the footwall of the GF fault in the Forezan section (see point 5 on Fig. 5B) suggesting a westward migration of the depocenter after the deposition of S2a. This is supported by thick maximum flooding deposits of S2b along the Chambéry syncline (i.e., 50 m-thick in section 5, contrasting with only 5 m thick to the east in section 4, Kalifi *et al.* 2020; Fig. 5B for localization). This is also in accordance with the first occurrences of decimeters thick interstratified conglomeratic levels within the S2b regressive deposits of section 5 (Fig. 5B) and the

sandy-dominated river-to-tidal deposits recorded in section 3 (Fig. 5B), arguing for a tectonically-controlled progradation of proximal deposits. To the south, in the Lans-Provezyieux syncline (see points 9, 10 on Fig. 5B), the "Voreppe palaeo-delta" (*sensu* Latreille 1969) was still active.

To the west, on the WSM Palaeohigh (~median domain; blue points on Fig. 5B), the S2b succession is dominated by sandy deposits of proximal marine environments. Transgressive deposits start with thin sandy limestones (0.5-5 m), still rich in *P. Praescabriusculus*, or by subtidal dunes showing ~NNE-SSW seaway-axis palaeo-currents (see point 20 on Fig. 5B). Those transgressive sediments are overlain by thin distal marine deposits, and this may still be linked with the influence of the WSM Palaeohigh. In the Bas-Dauphiné, the S2b seaway is bordered to the west by the MLP alaeohigh and the IC Palaeohigh. To the south, the Royans syncline and the Crest basin are then totally flooded. In the south of the Royans syncline (see point 35 on Fig. 5B), transgressive deposits of the S2b exhibit *P. Praescabriusculus*-rich calcarenites (0.5-5m), whereas 4km to the north of the Royans syncline, those deposits evolve towards *P. Praescabriusculus*-rich sandy subtidal dunes (see point 34 on Fig. 5B) and azoic sandy subtidal dunes (see point 32 on Fig. 5B). In the Royans syncline, the substratum on which the transgression occurred therefore evolves from south to north between upper Cretaceous limestones and fluvial sands of Oligocene age, respectively, and suggest that Miocene calcarenites facies mainly developed on a rocky substratum. This also explains why S2b deposits are characterized by fine-grained deposits only (“St-Lattier” marls) in the VAF1, VAF2, SLF1, SL1, SL2, SLF2, SLF3 and MO2 well-log data, as S2b deposits overlie either S2a or Oligocene fine-grained deposits. Similary, the “St-Lattier” marls unit that outcrops in the Royans syncline (see points 32, 34, 35 on Fig. 5B) consists of offshore, to offshore transition, depositional environments characterized by very fine-grained sandy to marly deposits (FA1, FA2, *sensu* Kalifi *et al.* 2020). Regressive deposits are characterized by open-coast subtidal to intertidal sandy deposits (FA5 to FA6, *sensu* Kalifi *et al.* 2020) suggestive of a deltaic progradation. To the west in BMT-1, MO-1, MO-3, PA-1 well-logs, S2b is mainly represented by sands, which were likely deposited in a deltaic environment (Fig. 5B) and implied the influence of fluvial inputs from the nearby exhumed terranes. Therefore, in the occidental domain, the location of the western Miocene coast during S2b was located close to the Massif Central in the south, and likely coincided with the ML Palaeohigh and IC Palaeohigh in the north.

The Langhian (S3 and S4) – Onsets of FZ3 and FZ4

The Langhian deposits are characterized by two depositional sequences: S3 and S4. During the deposition of these sequences, the oriental domain located to the east of the FZ2 was probably uplifting (Fig. 6), since no S4 deposits were observed in this area.

The S3 sequence: 16.2 to 15.0 Ma. The S3 transgression occurred at 16.3 +/- 0.3 Ma, 16.15 +/- 0.4 Ma, 16.5 +/- 0.25 Ma, 16.2 +/- 0.45 Ma and 16.7 +/- 0.25 Ma for zones A, C, E, G, and L, respectively (Figs. 1B and 2C; Kalifi *et al.* 2021), which matches the +35m T-6 eustatic transgression starting at ~16.2 Ma (Fig. 2B). The S3 sequence recorded the ongoing activity of FZ2 and thus, the continuous advance of the Belledonne basal thrust, as suggested by an abnormally thick S3 sequence at the footwall of FZ2 (Fig. 6A). The onset of FZ3 is, however, not so well constrained, but probably occurred during the deposition of S3 sequence (Kalifi *et al.* 2021).

During the S3 transgressive tract, the oriental domain recorded proximal deltaic deposits belonging to the river-to-tide transition zone (see points A4, 4, A8, A9, 5 on Fig. 6A). Conglomeratic levels indicate westward-directed palaeo-currents ("Chamoux conglomerate" unit, *sensu* Lamiraux 1977). The end of the conglomeratic succession does not outcrop. Directly to the west, above the WSM Palaeohigh in the median domain, the S3 deposits have embedded a different signature compared to

those from the oriental domain and are even distinct between the three zones constituting the median domain itself. To the north, in the Novalaise syncline, S3 sediments are characterized by thin transgressive deposits (5 to 20m) made of subtidal channels (see point 13 on Fig. 6A) and dunes, or by decimeters thick oyster-rich bioclastic limestones. This unit is then overlain by thick distal marine deposits (i.e. ~200m, section 13, Fig. 6A) corresponding to the S3 maximum flooding deposits (see points C4, 13, C6, 27, C9 on Fig. 6A). The lateral facies transition between distal marine sediments to the west (median domain) and proximal deltaic to the east (oriental domain) reflects the tectonically-driven uplift of the oriental domain (Fig. 6A) to the east of FZ2. This also indicates that the western part of the WSM Palaeohigh now corresponded to a highly subsiding area during the deposition of S3, as thick accumulations were recorded there. In the second zone constituting the median domain, to the north, in the La Pesse syncline (see point C1 on Fig. 6A), the sedimentary succession is different above the basal (oyster-rich) bioclastic transgressive deposits of S3. The latter deposits are overlain by 67m-thick "Coîtes conglomerates" (*sensu* Charollais *et al.* 2006; see point C1 on Fig. 6A) that consist of stacked units of tidal-influenced coarse-grained sandstones rich in sub-rounded and bioperforated micro-conglomerates (mainly local in origin) and marine fauna (bioclasts). Those ~30m-thick normally-graded sandstone beds likely reflect the infill of subtidal channels (FA7 *sensu* Kalifi *et al.* 2020). This unit is overlain by ~30m of tidal-influenced silty clay deposits. Despite the richness in palynomorphs, reworked nannofossils and the scarceness in foraminifera (Charollais *et al.* 2006) all suggesting proximal marine environments, the overlying deposits most probably correspond to the maximum flooding deposits of S3. These sediments are subsequently overlain by lacustrine limestones, but the continuity with the underlying sediments does not outcrop well, rendering their dating difficult. In the La Pesse syncline (see point C1 on Fig. 6A), S3 is characterized by more marine proximal deposits (compared to the southern part of the Novalaise syncline, see points C4, 13, C6, C9 on Fig. 6A) likely capped by lacustrine deposits that highlight the subaerial exposure at the top of S3. These lateral facies variations therefore suggest that, during the deposition of S3, the eastern part of the Jura was experiencing a progressive subaerial exposure, in response to the FZ2 activity. This is consistent with the lower to upper Langhian southward sea retreat described in the Swiss Molasse basin, in the north of the study area (Garefalakis and Schlunegger 2019).

In the third zone constituting the median domain, close to the Isere valley in the Voreppe syncline (see points 20, 21, 22 on Fig. 6A), transgressive sediments are 5-10 m thick. There, maximum flooding deposits are characterized by 2 to 5m-thick fine-grained open-coast-subtidal deposits, which are overlain by ~20m of open-coast intertidal deposits finally capped by conglomerates deposited in river-dominated environments (respectively FA5, FA6 and FA10 *sensu* Kalifi *et al.* 2020). The conglomerates correspond to braided-river deposits feeding a delta, as marine influences are attested by the occurrence of rare bioperforated pebbles. To the south, in the Rencurel syncline (see points 24, 25 on Fig. 6A), transgressive and maximum flooding deposits are characterized by coarse-grained calcarenites overlain by conglomeratic levels typical of a braided river in a deltaic position. These conglomeratic units of the S3 regression near the Isere valley constitute the fossil record of the Voreppe palaeo-delta (see points 20, 21, 22, 23; 24, 25 on Fig. 6A).

To the west, in the occidental domain (green points on Fig. 6A), the Bas-Dauphiné basin was flooded. In the Royans syncline and the Crest Basin, transgressive deposits exhibit 5-10 m thick oyster-rich bioclastic calcarenites (see points L4, 35, 34 on Fig. 6A). To the north of the Royans syncline (see point 32 on Fig. 6A), this facies evolves into large-scale sandy-dominated subtidal dunes (FA7 *sensu* Kalifi *et al.* 2020). Again, this particularity is induced by the presence of the rocky MM Palaeohigh southwards, but now flooded, which favored the local development of calcarenitic sediments. Above it, maximum flooding deposits of S3 are represented by marly- to sandy sediments typical of offshore

and open-coast subtidal environments (FA1 and FA5 *sensu* Kalifi *et al.* 2020) in the occidental domain, except in the TE-1 and BEF-1 wells (Fig. 6A). In those wells, S3 deposits are represented by coarse sandy deposits exhibiting interstratifications with thin layers of pebble-conglomerate, thus suggesting a proximal source likely from the Massif Central. In the CL-1, LTP-F1, DP-108, GVA-1 and BMT-1 wells (Fig. 6A), the marly deposits gradually pass to sandstones at the top of S3, thereby arguing for a deltaic progradation as well as proximity to the coast.

The S4 sequence: 15.0 to 14.0 Ma. The S4 transgression occurred at 15.07 +/- 0.42 Ma and 15.1 +/- 0.35 Ma for zones F and G, respectively (Figs. 1B and 2C; Kalifi *et al.* 2021), which matches the +15 m T-7 eustatic transgression starting at ~15.0 Ma (Fig. 2B). The westward migration of the depocenter proceeded with, as a result, a depocenter now located at the footwall of FZ4, as inferred from growth strata relationships (Kalifi *et al.* 2021). This is further confirmed by the westward migration of the most distal marine deposits of S4, now located to the west of the ML Palaeohigh (Fig. 6B), which consist of clay-dominated sediments in the FA-1, BEF-1, TE1, DP.108, MO1, MO2 and MO3 wells (Fig. 6B). Adjacent to those fine sediments, sandy deposits are far more frequent and suggest deltaic shallower marine environments.

In the oriental domain, to the east of FZ2 (Fig. 6B), no S4 deposits were found, thus implying that the area was totally uplifted at that time, and that sediments were bypassing towards the subsiding areas westwards. This is further in accordance with the presence of coarse-grained deltaic sediments along the median domain (blue points on Fig. 6B). In the northern part of this domain, mixed river-to-tide sandy-dominated deposits (with interstratification of conglomerates) are recorded (see points 13, C5, C6, C7, C10 on Fig. 6B). Conversely, in the La Pesse syncline (see point C1 on Fig. 6B), no marine sedimentation was recorded contemporaneously to S4, thus confirming the sea retreat southwards.

In the median domain, near Grenoble, at the footwall of FZ2, the 100 to 150m-high Pont Demay cliffs located along the eastern border of the Voreppe syncline in the Chartreuse massif (see points 20, 21 on Fig. 6B), display the sedimentary succession of the S4-S5 sequences (Fig. 7A, B). The stratigraphic framework is well constrained by sedimentological sections 20 to 23 (Fig. 7A, C; Kalifi *et al.* 2021). The Pont Demay cliffs highlight three stacked Gilbert deltas (GD) prograding to the north, which attest a continuous, tectonically-driven, creation of accommodation and steep slopes (Ricketts and Evenchick 2007) related to the FZ2 activity: the GD1a and GD1b belonging to the S4 (~15.0 to ~14.0 Ma), and the GD2 belonging to the S5 (~14.0 to ~12.0 Ma) (Fig. 7C, D), respectively, observed in the southern (Fig. 7D, E, F) and northern Pont Demay cliffs (Fig. 7D, G, H). Correlation between the two cliffs is based on the general dip of about 20° towards the east (Fig. 7D).

Two sedimentary facies were observed in the Gilbert deltas: (i) the GD foresets (F20, FA11 *sensu* Kalifi *et al.* 2020) are made of coarse matrix-supported conglomerates displaying large-scale northward-directed tangential cross-beds dipping at 20 to 30°; (ii) the Gilbert delta topsets (F19, FA10 *sensu* Kalifi *et al.* 2020) consisting of massive clast-supported and frequently imbricated conglomerates displaying low-angle, sub-planar, multi-metric trough cross-beds and forming a stack of multi-decimeter to meter-scale sheet levels of various grain sizes. In both facies, the clasts consist of well-rounded pebbles to cobbles mainly composed of local sources (Cretaceous limestones) and rare exotic clasts suggesting an internal alpine origin (e.g., radiolarites).

In the southern Pont Demay cliffs, the GD1a typifies the S4 boundary as it overlies planar-stratified conglomerates corresponding to regressive braided-fluvial deposits of S3 (Fig. 7C). S4 exhibits a 65 m-high depositional system of polyphased GD: GD1a and GD1b reaching 25 and 40 m in thickness, respectively (Fig. 7E). GD1a is characterized by northward prograding foresets as inferred from the

migration of planar-stratified conglomerates corresponding to braided fluvial deposits from a proximal deltaic position (Fig. 7E). The topsets of the GD1a are then overlain by the GD1b foresets that suggest a rapid retrogradation followed by another prograding unit. Again, the GD1b foresets exhibit a northward migration of the deltaic system. The transition between the ~35 m thick GD1b topsets (against only ~10 m for the GD1a) and the GD2 attributed to S5 (Fig. 7G) likely coincide with the T-8 eustatic transgression (Fig. 2B). In this interpretation, the GD1b topsets correspond to the topmost deposits of S4. In the orthogonal section (Fig. 7F), the GD1 foresets are planar-stratified, thus confirming the progradation of 2D sedimentary bodies. Note the growth-strata relationships in the GD1 topsets (Fig. 7F), in accordance with the tectonically-controlled stacking pattern of GD1a and GD1b during the deposition of S4, linked to the FZ2 activity.

The Serravallian (S5a-S5b and S6) – Onset of FZ5 and end of the P2?

Serravallian deposits were observed in the occidental and median domains (respectively green points and blue points, Fig. 8), and are characterized by three depositional sequences: S5a, S5b and S6. At that time, the oriental domain located to the east of FZ2 is likely subaerially exposed (Fig. 8), since no S5 deposits occurred in this area.

The S5a-S5b sequence: ~14.0 Ma to ~12.0 Ma. The S5a-S5b sequences were essentially constrained stratigraphically between the sequences S4 and S6. Well-log diagraphies indeed commonly exhibit two depositional sequences (S5a and S5b), which are most probably tied with the T-8 for the S5a (14.0 Ma), and the T-9a (13.2 Ma), T-9b (12.8 Ma) or even the T-10a (12.6 Ma) for S5b (Fig. 2A, B). The difficulty in matching S5b to the eustatic curve is due to minor sea-level changes (from only +/- 15 m; Fig. 2B) and, more generally, to the lack of accurate ages for S5a and S5b. The latest tectonic activity related to the Belledonne basement thrust advance is likely recorded during the deposition of S5a and S5b, which involved the activation of FZ5 (Kalifi *et al.* 2021) with a S5 depocenter localised at the FZ5 footwall.

During the transgressive phase of S5, the most distal facies in the occidental domain (green points on Fig. 8A) are still found to the west of the ML Palaeohigh, with a predominant clayey sedimentation in the FA-1, BEF-1, TE-1, DP-108 wells (Fig. 8A). Except for those wells, the S5 is characterized by sandy deposits in the Bas-Dauphiné basin, characteristic of tidal-influenced shallow-marine environments (see points K9, K11, 32 on Fig. 8A). In the K9 and K11 localities (Fig. 8A), metric to multi-metric high tidal dunes prograding to N 40° to 50° suggests palaeo-currents along the seaway axis. On the western border of the Bas-Dauphiné basin (see points K7, K10 on Fig. 8A), earlier studies have reported sands containing granitic clasts originated from the Massif Central (Latreille 1969), thus confirming the influence of fluvial inputs from a western relief. To the east, the median domain (blue points on Fig. 8A) is characterized by thick conglomeratic units deposited in river-dominated environments (see points C5, C7, C8 on Fig. 8A) which argue for uplifted areas eastwards. Coevally, in the northern part of the Isere valley, the stacked GD system of the Pont Demay terminated during the deposition of S5 (see points 21, 22 on Fig. 8A). Unlike for the GD1 of S4, the northward prograding GD2 developed during S5 is smaller in size (20 m high) and exhibit an abrupt transition between foresets and topsets (Fig. 7G, H), which suggests the final shallowing-up succession of the GD stacking pattern. Indeed, the topsets of the GD2 correspond to ~10m-thick planar-stratified conglomerates interpreted as braided-fluvial deposits. GD2 topsets are overlain by ~5m-high foresets prograding northwards (Fig. 7G, H). The lateral continuity of these foresets rules out the possibility that these structures correspond to interstratified bodies within the braided-fluvial system. Thus, we interpret these foresets as mouth bars in a distal deltaic position, that would plead for a final transgression corresponding to S5b. This unit is finally overlain by 50m of planar-stratified

conglomerates interpreted as braided-fluvial deposits (Fig. 7G, H). From the base to the top, the S5 succession infers (i) an upward decrease of slope and accommodation (of tectonic origin), or (ii) the still active FZ2 that induced a progressive exhumation of the deltaic environment.

The S6 sequence: ~12.0 to ~10.8 Ma. The S6 transgression occurred at 11.55 +/- 0.85 Ma and 11.7 +/- 0.8 Ma for zones L, J, respectively (Figs. 1B and 2C; Kalifi *et al.* 2021), and coincides with the T-10b eustatic transgression starting at ~12.0 Ma (Fig. 2B). During the deposition of S6, no tectonic activity was recorded in the occidental domain as inferred from S6 deposits isopach map in the Bas-Dauphiné basin (Kalifi *et al.* 2021). Furthermore, no growth strata relationships occur in S6 deposits, although growth strata were reported for S4 and S5 in the 91CHA1-2 seismic profile (Kalifi *et al.* 2021). To the east, in the median and oriental domains, the absence of S6 deposits does not allow to discuss the influence of tectonic activity.

In the occidental domain (green points on Fig. 8B), S6 was mainly described in well-logs. Transgressive S6 deposits are mainly characterized by bioclastic-rich sandstones (corals, bivalves, benthic foraminifera), which accumulated during the +40 m sea-level rise of the T-10b (Fig. 2B). The most pronounced Miocene transgression initiated the flooding of the La Bresse basin (Fig. 8B), as this domain had remained isolated from the Bas-Dauphiné basin since the beginning of the Miocene due to the Vienne Chamagnieu palaeo-high (VC Palaeohigh, Fig. 8B). Beyond the VC Palaeohigh, the S6 transgression probably invaded the study area even further north, since typical Miocene marine fauna was discovered up to latitudes equivalent to Lons-le-Saunier (120 km north of Lyon, Demarcq 1970 and references therein). Regressive deposits are characterized by shallow-marine sands that deposited widely in the study area, except in the eastern border of the Bas-Dauphiné basin (and probably in the median domain), where braided-fluvial environments predominated (PA-1, F2, LTPF-1, Fig. 8B). Two main fluvial systems are identified in this area: (i) the still active Voreppe delta downstream to the Isère valley, typified by the "Voreppe conglomerates" (VC, Fig. 8B) containing Mesozoic limestones and rare exotic clasts from the internal Alps including the Pelvoux massif (Bocquet 1966); (ii) the "La-Tour-du-Pin conglomerates" (LTPC, Fig. 8B) in the northern part of the Bas-Dauphiné basin, which contain granites from the Mont-Blanc massif and indicates south-west directed palaeocurrents (Nicolet 1979).

The Tortonian (S7 et S8) – Regional uplift and onset of the Jura frontal thrust:

Upper Serravallian and Tortonian deposits are observed in the occidental domain and the La Bresse domain (respectively, green and yellow points on Fig. 8C, D). These deposits are characterized by two depositional sequences: S7 and S8. During the deposition of these sequences, the median and oriental domains located to the east of FZ3 were likely already uplifted, since no deposits of this age have been described (Fig. 8C, D). In accordance, a new tectonic phase characterized by a regional uplift has been identified during the regressive phase of S7 and the deposition of S8 at ~10 Ma (phase P3, Fig. 2D), which induced the final retreat of the Miocene Seaway (Kalifi *et al.* 2021) coevally with the onset of the Jura thrust ("J" in Figs. 1B, 2C and 8D). Earlier chronostratigraphic studies based on Neogene mammals have indeed reported that the activity of the Jura front likely started between the Serravallian (~11 Ma) and the Pliocene (Bolliger *et al.* 1993; Steininger *et al.* 1996; Kälin 1997), as also inferred from U-Pb ages in syntectonic calcite mineralizations (Smeraglia *et al.* 2021).

S7 sequence: ~10.8 to ~9.5 Ma. The S7 transgression occurred at 10.6 +/- 0.7 Ma for zone I (Figs. 1B and 2C; Kalifi *et al.* 2021) and matches with the T-11 eustatic rise (+10 m) documented at ~10.8 Ma, just after the T-10b rapid -30 m sea-level fall (Fig. 2B). The la Bresse basin was still flooded during S7 judging from Strontium ages obtained in the I2, I17, I18 and I19 localities (Fig. 8C; Kalifi *et al.*

2021), as well as magnetostratigraphical and biostratigraphical dating within the Jujurieux section (I2 locality, Aguilar *et al.* 2004).

In the western part of the occidental domain (green points on Fig. 8C) and in the La Bresse basin, S7 transgressive deposits are characterized by tidally-influenced shallow-marine sandstones. Alternatively, the western border of the La Bresse, Bas-dauphiné and Crest basins was influenced by fluvial inputs from the Massif Central. Because no offshore marine deposits were recorded in this study area, maximum flooding deposits of S7 most likely correspond to subtidal deposits, especially in the central part of the basin (see point K4 on Fig. 8C). Such deposits are the last marine sediments recorded for the Miocene in this zone, since regressive deposits are characteristic of brackish, river-to-tide and river-dominated depositional environments.

In the eastern part of the occidental domain, S7 is either characterized by river-dominated deltaic sandstones or by aggrading conglomerates from the Voreppe and La-Tour-du-Pin deltas (VC, LTPC, Fig. 8C) that most probably merged in a single fan delta at that time.

S8 sequence: ~9.5 to ~8.2(?) Ma. S7 is directly overlain by continental deposits in the whole area (Fig. 2A). S8 deposits were dated based on mammal remains indicating ages ranging between ~9.5 and ~8.2 Ma (Kalifi *et al.* 2021 and references therein), therefore synchronously with the T-12 +25 m eustatic rise starting at ~9.5 Ma (Fig. 2B). The absence of marine deposits was interpreted as the response to the regional uplift involved by phase P3 (Fig. 2D). During this phase, the Jura thrust was active and involved a tectonically controlled depocenter at the footwall of that thrust (Kalifi *et al.* 2021), characterized by a 200 m-thick continental succession (consisting of lacustrine or alluvial plain deposits, Demarcq 1970). In the Bas-Dauphiné basin (F, H, J, K, L zones, Fig. 1B), the S8 is characterized by the progradation of river-dominated depositional systems, with sedimentary successions dominated by conglomerates deposited in braided-fluvial environments. Locally, the conglomerates are interstratified with fine-grained fluvio-lacustrine deposits rich in mammals and continental gastropods (see points H9, F5, K2 on Fig. 8D).

Palaeogeographic reconstructions of nearby areas

The lower Miocene chronostratigraphy of the Swiss Molasse Basin

Upper Aquitanian marine deposits (22.0 to 20.5 Ma, ~S1a; Berger *et al.* 2005) were never described northward from the city of Lausanne (Fig. 9). There, marine deposits rich in marine fauna were dated to the upper Aquitanian (Berger 1985; Kempf *et al.* 1999; Becker *et al.* 2010) and are interstratified within continental deposits at the top of the Lausanne "Molasse Grise" (Bersier 1936, 1938). Such interstratified marine and continental deposits were also observed for the S1a transgression (~21.0 Ma) in the southern prolongation of the Swiss Molasse basin (zone A of the study area on Fig. 4), which suggests a marine connexion between the two regions. No Aquitanian marine deposits were, however, described further north in the Rhine graben, the Swiss Jura or in the La Bresse basin, where Aquitanian deposits systematically consist of lacustrine or continental sediments (Becker 2000; Becker *et al.* 2004, 2010; Picot *et al.* 2008; Roussé *et al.* 2016). Hence, we advocate for an Aquitanian transgression originating from the south, as proposed by Berger *et al.* (2005).

In the Swiss Molasse basin (Fig. 9), a marine transgression is reported during the lower Burdigalian, at ~20.5 Ma (Berger 1985; Schlunegger *et al.* 1996, 1997; Kempf *et al.* 1999; Von Hagke *et al.* 2012; Jost *et al.* 2016), which matches well with the S1b transgression of the study area starting at ~20.6 Ma (Fig. 2A, B). In the Swiss Molasse basin, this lower Burdigalian transgression was diachronous and occurred from the SW to the NE (Garefalakis and Schlunegger 2019), which is also consistent with a

transgression originating from the south. Still in the Swiss Molasse basin, the upper Burdigalian recorded a tectonic phase affecting the entire Jura (Ziegler and Dèzes 2007). This phase is related to isostatic adjustments (induced by a tectonic pulse) generated by the exhumation of the Aar Massif (Garefalakis and Schlunegger 2019) that started around 20 Ma (Herwegh *et al.* 2017). The entire Swiss Molasse basin was thereafter exposed aerially, as evidenced by an angular unconformity reported between 18.3 and 17.8 Ma (Kempf *et al.* 1999; Garefalakis and Schlunegger 2019), and subsequently flooded by a marine transgression (Homewood 1981; Allen 1984). As a consequence, the latter transgression is accompanied by a drainage reversal, which was directed to the northeast during the lower Burdigalian, then redirected to the southwest during the late Burdigalian (Berger *et al.* 2005; Garefalakis and Schlunegger 2019). Such a tectonic phase, coeval to the upper Burdigalian marine transgression, precisely coincides with the S2a transgression in the study area (~17.8 Ma), which also records the onset of the Belledonne basal thrust (Fig. 5A). In the northern part of the Swiss Molasse basin (400 km north-east to Lausanne), a southward seaway retreat occurred between 17 and 16.5 Ma and was probably controlled by tectonic activity (Pippèrr and Reichenbacher 2017; Sant *et al.* 2017). Finally, during the lower Langhian, the Swiss Molasse basin deposits recorded the end of the southward-directed retreat of the Miocene Sea (16.0 to 15.0, Berger *et al.* 2005; ~S3).

The lower Miocene chronostratigraphy of the Rhodano-Provencal Molasse basin (RPMB)

The absence of Aquitanian marine deposits (S1a) to the north of the Swiss Molasse basin suggests a transgression from the south, through the Rhône valley and/or along the sub-alpine front more eastwards. The following section proposes a review including 19 localities from the RPMB (Fig. 9), combined with new Strontium dating carried out in the Valréas basin.

To the east of the RPMB, Aquitanian (~S1a) and lower Burdigalian (~S1b-c) marine deposits were recorded along the Arc de Castellane from the south (Nice) to the Digne basin (north) (Fig. 9). There, the seaway was limited to the east by palaeoreliefs (Bigot-Cormier *et al.* 2000; Bernet and Tricart 2011), as in our study area with FZ1 acting as a palaeotopographical barrier. At Roquebrune-Cap-Martin, on the south-eastern edge of the "Arc de Nice", (see point 1 on Fig. 9), lower Burdigalian deposits were also described (~S1b-c) (Laworsky 1959; Laworsky and Curti 1960; Feugueur and Le Calvez 1961). In the Vence syncline, in the southwestern edge of the Arc de Nice (see point 2 on Fig. 9), biostratigraphical studies allowed to date marine sediments to the Aquitanian (~S1a) (Odebode 1978, 1982; Campredon and Gigot 1984; Ginsburg *et al.* 1998) and lower Burdigalian (~S1b-c, Ginsburg and Mongin 1956; Mongin 1962; Odebode 1978, 1982). In St Vallier de Thiey, under the frontal overlap south of the Arc de Castellane (see point 3 on Fig. 9), marine sands have been attributed to the Tortonian (Dardeau *et al.* 2010). However, because they are located at the same latitude than the Vence syncline (see point 2 on Fig. 9), those sands rather suggest deposits belonging to the Aquitano-Burdigalian (~S1a-S1b-c). In the Majastres syncline to the west of the Arc de Castellane (see point 4 on Fig. 9), brackish deposits are intercalated between continental upper Oligocene and marine sediments (Espitalie 1964), hence most probably corresponding to the lower Burdigalian (Goguel 1936; Lapparent 1938). Such brackish deposits display benthic foraminifera assemblages similar to the "Digne Intermediate Molasse", which was dated to the upper Aquitanian (~S1a, see below), as well as some planktonic foraminifera including *G. ouachitaensis* (a marker of the upper Oligocene [+Aquitanian?]). At Châteauredon Dome (see point 5 on Fig. 9), continental deposits containing marine intercalations were dated to the Aquitanian (~S1a) by mammals (De Graciansky *et al.* 1982; Thome *et al.* 1989; Aguilar 2002) and isotopic data (Lopez *et al.* 2000; Bialkowski *et al.* 2006; Cojan *et al.* 2013). Isotope analyses have further confirmed a lower Burdigalian attribution, even if marine incursions are scarce (Lopez *et al.* 2000; Bialkowski *et al.* 2006). Under the Valensole plateau (see point 7 on Fig. 9), well-log data indicate a sedimentary

succession attributed to the Oligo-Aquitanian (marine?), which onlaps towards the west according to seismic imaging (Comité des Techniciens 1986). To the east, the closest wells to Digne (Mirabeau 1 - 2 and 3) possibly record the occurrence of Aquitanian deposits (Comité des Techniciens 1986). Such sediments are overlain by "Burdigalian *s.l.*" deposits that presumably suggest the lower Burdigalian (S1b-c). In the Digne basin (see point 6 on Fig. 9), within the "Digne Intermediate Molasse", the marine deposits were dated to the Aquitanian (~S1a) by marine fauna (Crumeyrolle *et al.* 1991) and Strontium dating (Largois 2000; Couëffé 2003; Rubino *et al.* 2015). The occurrence of the marine lower Burdigalian (~S1b-c) is well established by biostratigraphy (Haug 1891; Lapparent 1938; Haccard *et al.* 1989; Crumeyrolle *et al.* 1991) and Strontium dating (Largois 2000; Couëffé 2003). In those sedimentary successions, as in the underlying Aquitanian deposits, the influence of waves and storms (Rubino *et al.* 2015, 2019) indicates open coastal environments with large fetches.

To the west of the RPMB, Aquitanian deposits are continental in the Pertuis and Forcalquier synclines (Mein *et al.* 1971; Lesueur 1991; see points 8, 9 on Fig. 9), or even absent, as it is the case in the Baronnies synclines and in the Valréas basin (Rubino *et al.* 1990; Montenat *et al.* 2000). Marine Aquitanian deposits (~S1a) were indeed only described along the Mediterranean coast at Carry-le-Rouet (see point 12 on Fig. 9; Fontannes 1878; Catzigras 1943; Anglada 1972; Alvinerie *et al.* 1977; Anglada and Catzigras 1980; Demory *et al.* 2011), in the western border of the Nerthe area (see point 11 on Fig. 9; Dexcoté 2001), in the western border of the Camargue area along the Nimes fault (Demarcq 1970; Fig. 9) and in the Mediterranean offshore according to seismic and well log data (see points “off.1” [Bellaiche *et al.* 1976] and “off.2” [Fournier *et al.* 2016] on Fig.9). North of Carry-le-Rouet, the absence of marine lower Burdigalian deposits (~S1b-c) has been demonstrated (i) in the Nerthe area near Marseille, by a magnetostratigraphic study judging from a gap between ~19.9 to 18.5 Ma (see point 11 on Fig. 9; Oudet *et al.* 2010), (ii) in the north of the Basse Provence (Combaluzier 1932), (iii) in the Alpilles at Fontvieille (see point 13 on Fig. 9; Mongin 1949), as well as (iv) locally in the Valréas-Carpentras basin (Demarcq 1970; Rubino *et al.* 1990; Montenat *et al.* 2000). The Valréas basin is part of the RPMB and is located south of the Crest basin, the southernmost zone of the study area (Fig. 9, B for location). The lower Miocene stratigraphy of the Valréas basin has been revised, as detailed hereafter, in order to get a better understanding of the Miocene seaway palaeogeographical evolution at the scale of the Western Alpine foreland basin.

New Sr ages from the Valréas basin in the RPMB (lower Miocene)

Five new Strontium ages were obtained from the “St-Restitut” and “Nyons” sedimentological sections (Fig. 10A, D), and allow to integrate the stratigraphical scheme at a more regional scale by comparing it with the Royans and Crest basins located ~30-40km to the north (zones G and L respectively; Fig. 1B). In the “St-Restitut” and “Nyons” sections, the initial transgression was dated to 18.62 +/- 0.27 Ma and 18.87 +/- 0.32 Ma, respectively (Table 1). Such ages are rather homogeneous at the scale of the Valréas basin and coincide with the T-3b eustatic transgression described at ~19.0 Ma (Fig. 2B). This coincidence is, however, puzzling as the T-3b documents a +5m sea-level rise only. This transgression further matches with the S1c sequence described by Besson *et al.* (2005) in the RPMB. In our study area, the T-3b corresponds to the top of the S1b sequence (20.6 to 17.8 Ma), which generally poorly outcrops (sections 4, 5, Kalifi *et al.* 2020). Hence, unfortunately, the lack of detailed sedimentological sections for S1b prevents accurate sequence stratigraphical interpretations but does not rule out the possibility that another sequence (S1c) could fit with the T-3b transgression (Fig. 2 A, B).

Above the transgressive lag in the St-Restitut section (Fig. 10A), the S1c succession consists of large-scale tidal bars characterized by 5-10 m-high foresets prograding to the south (Lesueur *et al.* 1990)

and the S1c flooding was dated to 17.95 +/- 0.2 Ma (Fig. 10A). In the Nyons section (Fig. 10B), the S1c deposits are overlain by transgressive deposits constrained by a bioclastic-rich level dated at 17.60 +/- 0.25 Ma (Fig. 10B) and can be attributed to the S2a transgression.

Discussion

The previous palaeogeographical maps highlight to which extent the active Belledonne basal thrust shaped the Miocene seaway palaeogeographical evolution and the spatio-temporal distribution of sedimentary facies in the subalpine massifs, the southern Jura and the adjacent basins. The impact of this tectonic phase at the scale of the Western Alpine foreland basin will be further developed here, by integrating the lower Miocene seaway palaeogeographical evolution of the Swiss Molasse basin and the Rhodano-Provencal molasse basin (Fig. 9).

The origin of the upper Aquitanian transgression (S1a)

As marine upper Aquitanian deposits have only been described at Carry-le-Rouet (see point 12 on Fig. 9) and in the Digne and Vence basins along the Arc de Castellane (see points 1 to 6 on Fig. 9), the south-to-north Aquitanian transgression evidenced in this study likely followed a seaway that extended from the Vence sector near Nice (see point 2 on Fig. 9) to Lausanne in the north. To allow such a marine connection, the best candidate corresponds to the St-Disdier-en-Dévoluy syncline (see point 17 on Fig. 9), in which outcrop the St-Disdier sandstones attributed to the Oligocene. According to our investigations and the literature, the St-Disdier sandstones are continental in origin (Fabre *et al.* 1986; Meckel *et al.* 1996; Meckel 1997). Only the top of this unit consists of glauconitic sandy levels, which could represent possible candidates for marine deposits, however without other further pieces of evidence. The sedimentary succession of the St-Disdier sandstones is attributed to the upper Chattian based on the occurrence of diagnostic characeae (Fabre *et al.* 1986), which have also been recorded in the Forcalquier syncline (see point 8 on Fig. 9) within lacustrine Aquitanian deposits (Lesueur 1991). The upper Chattian of the St-Disdier Sandstones could therefore also be Aquitanian in age (Grosjean *et al.* 2017). Based on these elements, and the structural configuration of the early Miocene foreland basin characterized by a flexural subsidence at the footwall of the frontal thrusts (FZ1 in the north, Arc de Castellane in the south; Fig. 9), the most plausible hypothesis is a marine connection from the Digne basin in the south to the Lans-en-Vercors syncline (eastern edge of the Vercors) in the north throughout the St-Disdier-en-Dévoluy syncline (see point 17 on Fig. 9), in which early Miocene marine deposits would have been eroded today. Such a hypothesis has already been proposed for the Burdigalian seaway by Sissingh (2001) with the "Gap passage" connecting the Digne basin to the Vercors massif (Fig. 9). However, these works reported a marine connection between the Digne basin with the Rhône valley to the west, via the E-W the Baronnies passage, the Apt-Forcalquier and the Pertuis synclines (Fig. 9). In contrast, our new observations rather suggest that the early Miocene seaway was mainly connected via the Vence basin (Fig. 9) and the Ligurian Sea to the south-east, therefore suggesting a palaeogeography similar to the Lutetian/Priabonian 'foredeep' basin (Meulenkamp and Sissingh 2003; Ford *et al.* 2006; Lettéron *et al.* 2017) (Fig. 11A, B).

Our interpretation is further supported by the distribution of facies and depositional systems along the upper Aquitanian North-South seaway (Fig. 11A). In the Swiss Molasse basin, which constitutes the head of the embayment, the depositional environments are tide-dominated (Allen *et al.* 1985). Tide-dominated depositional environments run up to the southern Jura synclines, near Génissiat (see point 1 on Figs. 1B and 4; Berger 1985; Kalifi et al. 2021). To the south of the southern Jura synclines, depositional environments evolve into mixed wave-tide depositional environments (FA5, FA6, *sensu* Kalifi *et al.* 2020), while in the Digne basin (see point 6 on Fig. 11A), depositional environments are

wave-dominated (Fig. 11A; Crumeyrolle *et al*. 1990). In the Vence Syncline (see point 2 on Fig. 11A), open marine sediments characterized by marine marls rich in planktonic foraminifera (Odebode 1978, 1982) were deposited under the influence of both waves and tidal currents (Ginsburg *et al.* 1998). Such a process change from north to south is probably related to the degree of connection with the open marine Ligurian Sea to the south (Fig. 11A).

The Burdigalian (~20.6 Ma to ~16.2 Ma) paleogeography: Impact of an alpine-scale tectonic event

In the Valreas basin, our new results therefore invalidate the completeness of the lower Burdigalian stratotype section of Saint-Restitut (Fontannes 1878; Deperet 1892; Demarcq *et al.* 1974; Demarcq 1980), since Strontium ages clearly exhibit that the initial transgression only occurred at the end of the lower Burdigalian (~18.9 Ma, S1c sequence; see points 15, 16 on Fig. 11C). This is further in line with the end of the gap reported from the Nerthe area, which was dated to approximately 18.5 Ma, and that preceded a return to marine conditions (Oudet *et al.* 2010; see point 11 on Fig. 11C). On both sides of the Luberon massif, in the Pertuis syncline (see point 9 on Fig. 11B, C; Mein *et al.* 1971) and in the Forcalquier syncline (see point 8 on Fig. 11B, C), mammals ages further outline that lower Burdigalian deposits indeed corresponded to non-marine deposits (lacustrine or deltaic; Lesueur 1991). To the east, the early Miocene seaway still connect the Swiss molasse basin to the Vence area (see point 2 on Fig. 11C).

A connexion between the RPMB and the Bas-Dauphiné basin to the north is finally established during the Upper Burdigalian transgression (~17.8 Ma, Fig. 11D), through the Nerthe sector (see point 11 on Fig. 9; Oudet *et al.* 2010), the Camargue in the Basse-Provence (Fig. 9; Demarcq 1970), the Valréas Basin (Fig. 9; Lesueur *et al.* 1990) and the Crest and Royans basins (Fig. 5) to the south of the study area. Eastwards, the Apt-Forcalquier synclines (see points 8, 10 on Fig. 9; Gigot *et al.* 1982) and the Baronnies passage are also flooded during the Upper Burdigalian (Guy *et al.* 1989), linking the Digne Basin to the east and the Rhône valley to the west (Fig. 11D). Even more to the east, in the Digne basin, the presence of the Miocene Sea is still reported during the Upper Burdigalian. From south to north, marine upper Burdigalian sediments have indeed been described in the Vence syncline (see point 2 on Fig. 9; Ginsburg *et al.* 1998) and under the Valensole plateau (see point 7 on Fig. 9; Comité des Techniciens 1986), as based on the presence of deltaic mouth bars arguing for coastal depositional environments. Marine Upper Burdigalian sediments have also been described in the Digne Basin (see point 6 on Fig. 9) where upper Burdigalian deposits are attested by mammals (Couëffé and Maridet 2003), even if not reported from the Velodrome section (Crumeyrolle *et al.* 1991; Rubino *et al.* 2015).

Thus, the Upper Burdigalian transgression (~17.8 Ma, Fig. 11D) records the flooding of the entire Rhône valley and allowed a much wider connexion between the RPMB and the SMB via the eastern Bas Dauphiné and the northern Subalpine ranges (Fig. 11D, E). These domains were flooded for the first time by passing over the WSM Palaeohigh (Fig. 5). Interestingly, such a connexion is precisely contemporaneous with the activation of the Belledonne basal thrust corresponding to the onset of the tectonic phase P2 (activation of the SAL thrust) described in the study area (Kalifi *et al.* 2021).

To the North, in the Swiss Molasse basin, the upper Burdigalian transgression (~17.8 Ma) was associated with an Upper Burdigalian tectonic phase triggering an inversion of drainage direction and affecting the entire Jura (Ziegler and Dèzes 2007). This tectonic phase precisely also coincides with the onset of phase P2 in the study area (~18.05 +/- 0.25 Ma). To the South, in the Rhodano-Provencal Molasse basin (RPMB, Fig. 1A), lower Miocene syntectonic deposits (Upper Burdigalian-Langhian; ~18-14 Ma) were described in the Digne area (Gigot *et al.* 1974; Beaudoin *et al.* 1975; Crumeyrolle *et*

al. 1991), in the Lubéron (Clauzon 1974), in the Alpilles (Colomb 1982) and in the Vaison-la-Romaine (Brasseur 1962), corresponding to the first Miocene alpine tectonic phase of the RPMB (Gigot *et al.* 1974). Thus, this RPMB tectonic phase precisely coincides with the onset of phase P2 in the study area (~18.05 +/- 0.25 Ma; Kalifi *et al.* 2021) and argues for a tectonic phase recorded at the scale of the western Alps. Therefore, the (upper Burdigalian) initial marine connexion between the Rhône valley and the Swiss molasse basin occurred coevally with an upper Burdigalian alpine-scale tectonic event (P2, onset at ~18.05 +/- 0.25 Ma; Kalifi *et al.* 2021), suggesting that the subsequent westward-directed migration of the Miocene seaway, the establishment of new marine connexions and the abandonment of former corridors (Fig. 11C) were all likely tectonically-controlled as well.

The Langhian to upper Tortonian (~16.2 Ma to ~9.5 Ma) palaeogeography

Upper Burdigalian tectonic episodes are rapidly followed by a southward-directed retreat of the Miocene seaway between 17 and 16.5 Ma (~S2b sequence) in the northern part of the Swiss Molasse basin (400 km north-east to Lausanne, Pippèrr and Reichenbacher 2017; Sant *et al.* 2017). Such a retreat is finally recorded in the southern part of the Swiss Molasse basin during the lower Langhian (16.0 to 15.0, Berger *et al.* 2005; ~S3 sequence; Fig. 11E). Pippèrr and Reichenbacher (2017) and Sant *et al.* (2017) suggest that the seaway retreat is controlled by tectonic activity; this seems consistent with the emerging activity of the SAL, GF and FZ2 faults during phase P2 in the study area (Fig. 6A), where the westward-directed migration of the seaway is still in progress as the entire Bas-Dauphiné basin is totally flooded for the first time (Fig. 11E). However, the westward migration of the seaway is attested by the persavive migration of depocenters to the west from the footwall of the SAL fault (~18 Ma to ~17.2 Ma) to the footwalls of the GF (~17.2 to ~16.2 Ma) and FZ2 faults (~16.2 to ~15 Ma; Kalifi *et al.* 2021), successively, thereby reflecting the in-sequence propagation of the thrusts. To the south, during the Langhian, syntectonic deposits are still recorded in the RPMB (Villegier 1984; Villegier and Andrieux 1987; Bergerat 1985).

Subsequently, between the Upper Langhian (~15.0 Ma, Fig. 11F) and the Lower Tortonian (~9.5 Ma, Fig. 11G), no major palaeogeographical change occurred. P2 is still active in the study area, until at least ~12.0 Ma (Figs. 6B, 7A and 11F). Then, the +40m sea-level rise recorded at ~12.0 Ma (S6 transgression; Fig. 2B) triggered the first marine transgression of the La Bresse basin above the Vienne-Chamagnieu Palaeohigh (Figs. 8B and 11G). In the RPMB, and despite such a notable sea-level rise, marine disconnections established during S4 and S5 (Fig. 11F) pursued between the Vence syncline and the Digne basin (see points 2, 6 on Fig. 11F), and between the Digne basin and the Valreas basin through the Baronnies passage (see points 6, 15, 16 on Fig. 11G; Montenat *et al.* 2000), thus suggesting a southwest-directed progressive seaway retreat triggered by uplifts.

Finally, during the Upper Tortonian, the S8 sequence highlights a rapid southward retreat of the Miocene sea (Figs. 8D and 11H) coeval to the onset of the tectonic phase P3 (activation of the Jura thrust; Fig. 2D), implying here again that sea retreat was tectonically-controlled. In the RPMB, this tectonic phase was also recorded (Lapparent 1940, 1941; Dubois 1966; Gigot *et al.* 1974; Villegier 1984; Villegier and Andrieux 1987). Nevertheless, marine conditions still prevailed in the RPMB during the Upper Tortonian (Besson 2005; Fig. 11H).

Conclusions

Based on a revised chronostratigraphy and tectonostratigraphy study from the subalpine massifs, the southern Jura and the adjacent basins, the elaboration of new palaeogeographical maps highlights the influence of active tectonics on seaway palaeogeographical evolution over the course of the Miocene.

During the upper Aquitanian to lower Burdigalian (~21.0 to 17.8 Ma), the initial Miocene marine transgression occurred along the active alpine orogenic front, by connecting the Digne basin to the south and the Swiss Molasse basin to the north. In the study area, the Miocene seaway was influenced by flexural subsidence and restricted between the FZ1 to the east and the Western Subalpine Massif Palaeohigh to the west. This narrow configuration, almost parallel to the alpine front (~NNE-SSW), involved an amplification of tidal currents, as highlighted by seaway-directed axes of subtidal dunes.

At 18.05 +/- 0.25 Ma, the eustatic transgression of S2a was sub-synchronous to the activation of the thick-skinned Belledonne basal thrust widely affecting this external part of the Alps (phase P2, *sensu* Kalifi *et al.* 2021). This phase lasted at least until ~12.0 Ma. The westward-directed in-sequence propagation of the thrusts implied the brutal westward migration of the Miocene seaway (and associated depocenters) from the oriental domain to the occidental domain. Between S2a and the end of S3 (~17.8 to ~15.0 Ma), the oriental domain evolved into a piggy-back basin and was progressively uplifted. Coevally, the median domain to the west, located on the inherited Western Subalpine Massif Palaeohigh, was flooded for the first time during the Miocene. During S3 (~16.2 Ma), the seaway definitively invaded the occidental domain and extended as far as to the Massif Central westwards. Between the oriental and the occidental domains, the median domain evolved into a piggy-back basin, but still subsided until at least S5 (~12 Ma).

During the first stage of the seaway westward migration (S2a, S2b, S3; ~17.8 to ~15.0 Ma), the median domain exhibited important lateral facies variations resulting from inherited palaeotopographies. Incised valleys along the Western Subalpine Massif Palaeohigh favored the development of tide-dominated environments by local flow constriction, which even more amplified the tidal amplification involved by the narrow seaway configuration (Kalifi *et al.* 2020). In turn, coarse-grained deposits linked to fluvial input originating from the active orogenic wedge prevailed in the eastern coast, as evidenced by stacked Gilbert deltas highlighting a continuous tectonic-driven creation of slope and accommodation during S4 and S5 (~15.0 to ~12.0 Ma).

At the scale of the Western Alpine foreland basin, the Belledonne basal thrust involved: (1) the flooding of the Rhône valley and the initiation of a marine connection between the Swiss molasse basin to the north and the Rhodano-Provencal molasse basin to the south; (2) the initiation of the progressive southward retreat of the Miocene seaway from the Swiss Molasse basin, which was definitively disconnected from the seaway between S3 and S4 (~16.2 to 14.0 Ma).

This revised palaeogeographical reconstruction of the Miocene Western Alpine seaway thus demonstrates how much eustatic-driven depositional zones are impacted by tectonics over the course of alpine deformation, and provides a valuable model of the evolution of seaway palaeogeographical configuration in foreland basins, and the associated changes in depositional environments under the influence of dominant hydrodynamic processes.

Acknowledgements

The authors would like to thank TOTAL for the financement of this PhD study. We would like to thank Philippe Grandjean, Romain Grime, Thomas Pichancourt, Hawoly Bass, Astrid Jonet, Antoine Mercier, Alessandro Menini, Pierre and Thomas Courrier, Daniel Fournier, Ludovic Mocochain, Sidonie Revillon, Hugues Fenies, Loïc Costeur, Jonathan Pelletier, Edouard Le-Garzic, Xavier Du-Bernard, Jean-Pierre Girard and Francois Lafont for their precious help in the field and/or for fruitful discussions. Constructive reviews by Jean-Yves Reynaud and Dan Palcu helped to improve the manuscript.

Author contributions

This study was performed by AK in the framework of his Ph.D, co-supervised by TOTAL (CSTJF, Pau, France) and the LGL-TPE (University Lyon 1). JLR conceptualized the original research topic of this study, with the support of VS, in the EXPLO/EP/GTS/ISS entity of TOTAL. The palaeogeographical maps were drawn by AK under the supervision of PS, BP, JLR and PHL. The sampling and the sample preparation for the chemostratigraphical study was achieved by AK, and the analysis and interpretations were conducted by AG. The VRGS model of the stacked-gilbert deltas was performed by SR, and the interpretations was proposed by SR, BH and AK. AK wrote the paper, with major contributions of PS, BP and JLR, and corrections from all other co-authors. The authors would also like to pay a special tribute to Bernard Pittet who recently passed away and who contributed greatly to this study.

Funding

The authors would like to thank TOTAL for the financement of this PhD study.

Data availability

All data generated or analysed during this study are included in this published article.

References

Aguilar, J.P. 2002. Biochronologie des localités de mammifères du Sud-Est de la France. *In*: Besson, D., Clauzon, G., Coueffe R., Dexcoté Y., Ferry S., Jimenez-Moreno G., Parize, O. Rubino J.L., Suc J.P. and Tessier B. (eds) *Le Néogène Du Bassin d'avant-Pays Rhodano-Provençal, Field-Trip Stati2002 Guidebook*, Soc. Géol. France Library.

Aguilar, J.P., Bergreen, W.A., Aubry, M.P., Kent, D.V., Clauzon, G., Bennami, M., Michaux, G. 2004. Mid-Neogene Mediterranean marine-continental correlations: an alternative interpretation, *Palaeogeography, Palaeoclimatology, Palaeoecology*, **204**, 165-186.

Allen, P.A. 1984. Reconstruction of ancient sea conditions with an example from the Swiss Molasse. Marine Geology, **60**, 455–473.

Allen, P.A. and Bass, J.P. 1993. Sedimentology of the upper marine molasse of the Rhône-Alp Region, Eastern France: implications of basin evolution. Eclogae Geologicae Helvetiae, **86**, 121–172.

Allen, P.A., Mange-Rajetzky, M., Matter, A. and Homewood, P. 1985. Dynamic palaeogeography of the open Burdigalian seaway, Swiss Molasse basin. *Eclogae Geologicae Helvetiae*, **78**, 351–381.

Alvinerie, J., Carolp, M., Anglada, R. and Catzigras, F. 1977. *Stratotype et Parastratotype de l'Aquitanien*, Editions du CNRS, I.S.B.N. 2-222-021 40 5.

Anglada, R. 1972. Etude des petits foraminifères. *In:* Andreieff P., Anglada R., Carbonnel G., Catzigras F., Cavelier C., Chateauneuf J.J., Colomb E., Jacob C., Lai J., L'Homer A., Lezaud L., Lorenz C., Mercier H. and Parfenoff A. (eds), *V^e Congrès du Néogène méditerranéen, Vol. III, Contribution à l'étude de Carry-le-Rouet (Bouches-du-Rhône)*, Mémoires du BRGM, 1, **4**, 29–35.

Anglada, R. and Catzigras, F. 1980. Les étages français et leurs stratotypes - Aquitanien sj. (parastratotypes). *In* : Cavelier, C. and Roger, J. (eds) *Les étages français et leurs stratotypes*. *Mémoires du BRGM*, **109**, 264–268.

Bass, J.P. 1991. *The Sedimentology and Basin Evolution of the Upper Marine Molasse of the Rhône-Alp Region, France*. Ph.D. Thesis, Department of Earth sciences, University of Oxford.

Beaudoin B., Campredon R., Cotillon P. and Gigot P. 1975. Alpes Méridionales Françaises : Reconstitution du bassin de sédimentation, Excursion N°7, *IX Congrès International de Sédimentologie*, Nice, IAS Publ.

Becker, A. 2000. The Jura Mountains—an active foreland fold-and-thrust belt?. *Tectonophysics*, **321**, 381–406.

Becker, D., Lapaire, F., Picot, L., Engesser, B. and Berger, J.-P. 2004. Biostratigraphie et paléoécologie du gisement à vertébrés de La Beuchille (Oligocène, Jura, Suisse). *Revue de paléobiologie*, **9**, 179–191.

Becker, D., Antoine, P.O., Engesser, B., Hiard, F., Hostettler, B., Menkveld-Gfeller, U., Mennecart, B., Scherler, L., Berger, J.P. 2010. Late Aquitanian mammals from Engehalde (Molasse Basin, Canton Bern, Switzerland). *Annales de Paléontologie*, **96**, 95–116, https://doi.org/10.1016/j.annpal.2011.03.001.

Belknap, D.F. and Kraft, J.C. 1985. Influence of antecedent geology on stratigraphic preservation potential and evolution of Delaware's barrier systems. *Marine geology*, **63**, 235–262.

Bellahsen, N., Mouthereau, F., Boutoux, A., Bellanger, M., Lacombe, O., Jolivet, L. and Rolland, Y. 2014. Collision kinematics in the western external Alps. *Tectonics*, **33**, 1055–1088.

Bellaiche, G., Irr, F. and Labarberie, M. 1976. Découverte de sédiments marins finis-oligocènes et aquitaniens au large du Massif des Maures (canyon des Stoechades). *C. R. Acad. Sci., Paris*, D, **283**, 319–322.

Berger, J.P. 1985. La transgression de la molasse marine supérieure (OMM) en Suisse occidentale. *Munchn. geowiss. Abh. Reihe A. muenchen*, **5**, 1-208.

Berger, J.P., Reichenbacher, B., et Becker, D., Grimm, M., Grimm, K., Picot, L., Storni, A., Pirkenseer, C., Derer, C., Schaefer, A. 2005. Eocene-Pliocene time scale and stratigraphy of the Upper Rhine Graben (URG) and the Swiss Molasse Basin (SMB). *International Journal of Earth Sciences*, **94**, 711–731.

Bergerat, F. 1985. Déformations cassantes et champs de contrainte tertiaires dans la plate-forme européenne, PhD Thesis, Université Pierre et Marie Curie-Paris VI.

Bergerat, F. 1987. Paléo-champs de contrainte tertiaires dans la plate-forme européenne au front de l'orogène alpin. *Bulletin de la Société géologique de France*, **3**, 611–620.

Bergerat, F., Mugnier, J.-L., Guellec, S., Truffert, C. and Cazes, M. 1990. Extensional tectonics and subsidence of the Bresse basin: an interpretation from ECORS data. *Mémoires de la Société géologique de France*, **156**, 145–156.

Berne, S., Auffret, J. and Walker, P. 1988. Internal structure of subtidal sandwaves revealed by high-resolution seismic reflection. *Sedimentology*, **35**, 5–20.

Bernet, M. and Tricart, P. 2011. The Oligocene orogenic pulse in the Southern Penninic Arc (Western Alps): structural, sedimentary and thermochronological constraints. *Bulletin de la Société géologique de France*, **182**, 25–36.

Bersier, A. 1936. La forme de la transgression burdigalienne dans la région vaudoise. *Bull. Soc. Géol. France*, **20**, 111–114.

Bersier, A. 1938. Recherches sur la géologie et la stratigraphie du Jorat, *Mémoires de la Société vaudoise des sciences naturelles*, **6/3**, 1-128.

Besson, D., Parize, O., Rubino, J.L., Aguilar, J.P., Aubry, M.P., Beaudoin, B., Berggren, W.A., Clauzon, G., Crumeyrolle, P., Dexcoté, Y., Fiet, N., Iaccarino, S., Jiménez-Moreno, G., Laporte-Galaa, C., Michaux, J., Von Salis, K., Suc, J.P., Reynaud, J.Y., Wernli, R. 2005. Un réseau fluviatile d'âge Burdigalien terminal dans le Sud-Est de la France: Remplissage, extension, âge, implications. *Comptes Rendus Geoscience*, **337**, 1045–1054, https://doi.org/10.1016/j.crte.2005.05.009.

Besson, D. 2005. Architecture du bassin rhodano-provençal miocène (Alpes, SE France): Relations entre déformation, physiographie et sédimentation dans un bassin molassique d'avant-pays, Phd Thesis, École Nationale Supérieure des Mines de Paris.

Bialkowski, A., Châteauneuf, J.-J., Cojan, I. and Bauer, H. 2006. Integrated stratigraphy and paleoenvironmental reconstruction of the Miocene series of the Châteauredon Dome, SE France. *Eclogae Geologicae Helvetiae*, **99**, 1–15.

Bigot-Cormier, F., Poupeau, G. and Sosson, M. 2000. Dénudations différentielles du massif cristallin externe alpin de l'Argentera (Sud-Est de la France) révélées par thermochronologie traces de fission (apatites, zircons). *Comptes Rendus de l'Académie des Sciences-Series IIA-Earth and Planetary Science*, **330**, 363–370.

Bocquet, J. 1966. Le delta miocène de Voreppe. Etude des faciès conglomératiques du Miocène des environs de Grenoble. *Travaux du Laboratoire de Géologie de l'Université de Grenoble*, **42**, 53–75.

Bolliger, T., Engesser, B. and Weidmann, M. 1993. Première découverte de mammifères pliocènes dans le Jura neuchâtelois. *Eclogae Geol. Helv*, **86**, 1031–1068.

Brasseur R .1962. Etude Géologique du Massif de Suzette (Vaucluse), PhD Thesis, Université de Lyon, 195p.

Butler, R.W.H. 1992. Structural evolution of the western Chartreuse fold and thrust system, NW French Subalpine chains. *In*: McClay, K.R. (ed.), *Thrust Tectonics*, Chapman and Hall, 287–298.

Campredon, R. and Gigot, P. 1984. Le Néogène : bassin niçois et varois. *In* : Debrand-Passard, S., Courbouleix, S., & Lienhardt, M. J. (eds), *Synthèse géologique du Sud-Est de la France*, Mémoires du BRGM, 499–501.

Catuneanu, O. 2004. Retroarc foreland systems–evolution through time. *Journal of African Earth Sciences*, **38**, 225–242.

Catuneanu, O. 2019. First-order foreland cycles: Interplay of flexural tectonics, dynamic loading, and sedimentation. *Journal of Geodynamics*, **129**, 290–298.

Catzigras, F. 1943. L'Aquitanien marin de Carry-le-Rouet. *Annales de la faculté des sciences de Marseille*, **217**, 1-133.

Charollais, J., Wernli, R., Du Chene, R.J., Von Salis, K. and Steiner, F. 2006. La Molasse marine supérieure de la Combe d'Evuaz et de la Pesse. *Archives des sciences*, **59**, 21–46.

Clauzon G. 1974. Quel age le Lubéron a-t-il ? *Etudes Vauclusiennes*, **XI**, 1-16

Cojan, I., Bialkowski, A., Gillot, T. and Renard, M. 2013. Paleoenvironnement and paleoclimate reconstruction for the early to middle Miocene from stable isotopes in pedogenic carbonates (Digne-Valensole basin, southeastern France). *Bulletin de la Société Géologique de France*, **184**, 583–599.

Colomb E., 1982. Relation plate-forme carbonatée – continent dans le cas de la transgression Miocène dans les Alpilles (Bouches-du-Rhône). *Géologie Méditerranéenne*, **9**, 3, 213-215.

Combaluzier, C. 1932. Le Miocène de La Basse-Provence. *Services de la Carte géologique de France*, **35**, 1-170.

Comité des Techniciens 1986. *Corps Sédimentaires, Exemples Sismiques et Diagraphiques : Comité des Techniciens de la Chambre Syndicale de la Recherche et de la Production du Pétrole et du Gaz Naturel*, Ed. Techni. Paris.

Costeur, L. 2005. *Les communautés de mammifères d'Europe de l'Oligocène supérieur au Pliocène inférieur : paléobiogréographie et paléobiodiversité des ongulés, paléoenvironnements et paléoécologie évolutive*. Ph.D. Thesis, University of Lyon 1.

Couëffé, R. 2003. *La préservation du temps dans les enregistrements sédimentaires : analyse quantitative à l'intérieur de la molasse marine miocène du bassin d'avant-chaîne de Digne (Alpes de Haute Provence, sud-est de la France)*. Ph.D. Thesis, University of Caen.

Couëffé, R. and Maridet, O. 2003. Découverte de deux gisements à micromammifères du Burdigalien supérieur dans la molasse du bassin de Digne (Alpes de Haute Provence, SE France): implications stratigraphiques et tectoniques. *Eclogae Geol. Helv*, **96**, 197–207.

Crumeyrolle, P., Rubino, J. and Clauzon, G. 1991. Miocene depositional sequences within a tectonically controlled transgressive–regressive cycle. *In*: MacDonald, D.I.M. (ed.), *Sedimentation, Tectonics and Eustasy: Sea-Level Changes at Active Margins*, Spec. Publ. int. Ass. Sediment., **12**, 371–390.

Curial, A. 1986. *La sédimentation salifère et suprasalifère du Paléogène bressan (France): comparaison entre les données diagraphiques et lithologiques. Etude diagraphique du champ d'Etrez et synthèse du bassin.* Ph.D. Thesis, University of Lyon 1.

Dardeau, G., Dubar, M., Toutin-Morin, N., Courme, M.-D., Crévola, G. and Mangan, C. 2010. Notice explicative, Carte géol. France (1/50 000), feuille Grasse-Cannes (999). *BRGM*, 1-194.

Dasarathi, N. 1965. Etude geologique de la bordure occidentale du Vercors. *Géologie alpine*, **42**, 83–96.

De Graciansky, P.C., Durozoy, G. and Gigot, P. 1982. Notice explicative, Carte géol. France (1/50 000), feuille Digne (944). *BRGM*, 1-35.

De Weger, W., Hernández-Molina, F.J., Flecker, R., Sierro, F.J., Chiarella, D., Krijgsman, W. and Manar, M.A. 2020. Late Miocene contourite channel system reveals intermittent overflow behavior. *Geology*, **48**, 1194–1199.

Debelmas, J. 1974. Géologie de la France : Les Chaînes plissées du cycle alpin et leur avant-pays. Editions Doin, **2**, 296-540.

DeCelles, P.G. and Giles, K.A. 1996. Foreland basin systems. *Basin research*, **8**, 105–123.

Defant, A. 1961. Physical Oceanography, vol. 1. Pergamon Press, 1–598.

Demarcq, G. 1959. Le Miocene du bassin de Crest (Drome). *Bulletin de la Société Géologique de France*, **7**, 93–100.

Demarcq, G. 1970. Etude stratigraphique du Miocène rhodanien. *Mém. BRGM.*, **61**, 1–257.

Demarcq, G. 1980. Le Stratotype du Burdigalien. *In* : Cavelier, C. and Roger, J. (eds) *Les étages français et leurs stratotypes*. *Mémoires du BRGM*, **109**, 272–278.

Demarcq, G., Magne, J., Anglada, R. and Carbonnel, G. 1974. Le Burdigalien stratotypique de la Vallée du Rhône; sa position biostratigraphique. *Bulletin de la Société Géologique de France*, **7**, 509–515.

Demarcq, G. and Perriaux, J. 1984. Néogène. *In* : Debrand-Passard, S., Courbouleix, S. et Liehardt, M.J. (eds) *Synthèse géologique du sud-est de la France*. Mémoires du BRGM, 469–519.

Demarcq, G., Gourinard, Y. and Magné, J. 1989. Grade-datation dans le Burdigalien du bassin de Crest (Drôme, moyenne vallée du Rhône): comparaison avec le stratotype rhodanien. *Geobios*, **22**, 383–386.

Demory, F., Conesa, G., et al. 2011. Magnetostratigraphy and paleoenvironments in shallow-water carbonates: the Oligocene-Miocene sediments of the northern margin of the Liguro-Provençal basin (West Marseille, southeastern France). *Bulletin de la Société géologique de France*, **182**, 37–55.

Depéret, C. 1892. Sur le parallélisme du système Miocène, *Bull. Soc. Géol. France.*, Paris, 3ème série, tome 20, 145-156.

Depéret, C. 1895. Aperçu sur la structure générale et l'histoire de la formation de la vallée du Rhône. *Annales de Géographie*, **4**, 432–452.

Dexcoté, Y. 2001. *Architecture et évolutions des facies des séquences de dépôts du Miocene de Basse Provence*. Master thesis, Université Pierre et Marie Curie.

Deville, E. 2021. Structure of the Tectonic Front of the Western Alps: Control of Fluid Pressure and Halite Occurrence on the Decollement Processes, *Tectonics*, **40**, 4.

Dickinson, R.W. 1974. Plate tectonics and sedimentation. *In:* Dickinson, R. W. (ed.) *Tectonics and Sedimentation*, Spec. Publ. of SEPM, 22, 1–27, https://doi.org/10.2110/pec.74.22.0001.

Doudoux, B., de Lepinay, B. M., and Tardy, M. 1982. Une interprétation nouvelle de la structure des massifs subalpins savoyards (Alpes occidentales): nappes de charriage oligocènes et déformations superposées. *CR Acad. Sci*, **295**, 63–68.

Dubois, P. (1966). Sur la sédimentation et la tectonique du Miocène de la Provence occidentale. *Bulletin de la Société Géologique de France*, **7**(6), 793-801.

Enay, R. 1980. L'île Crémieu. Evolution morphologique et structurale. *Publications de la Société Linnéenne de Lyon*, **49**, 482–505.

Embry, A.F. 1993. Transgressive–regressive (T–R) sequence analysis of the Jurassic succession of the Sverdrup Basin, Canadian Arctic Archipelago. *Can. J. Earth Sci.*, **30**, 301–320.

Embry, A.F. 1995. Sequence boundaries and sequence hierarchies: problems and proposals. *Seq. Stratigr. Northwest Eur. Margin*, **5**, 1–11.

Espitalie, J. 1964. *Contribution à l'étude du Tertiaire du Synclinal de Majastres (feuilles au 1/2000e, Digne 5-6, Moustiers-Sainte-Marie 1-2 et 3-4)*. DES, Univ J. Fournier (Grenoble).

Fabre, P., Médus, J. and Paris, J.-L. 1986. Caractérisation de l'Eocène et de l'Oligocène marins dans les chaînes subalpines méridionales à l'ouest de Gap (Hautes-Alpes, France). *Eclogae Geologicae Helvetiae*, **79**, 719–730.

Ferret, Y. 2011. *Morphodynamique de Dunes Sous-Marines En Contexte de Plate-Forme Mégatidale (Manche Orientale). Approche Multi-Échelles Spatio-Temporelles*. Ph.D. Thesis, University of Rouen.

Feugueur, L. and Le Calvez, Y. 1961. Presence du Miocene dans le" tunnel ferroviaire de Monaco", Alpes-Maritimes. *Bulletin de la Société Géologique de France*, **7**, 21–26.

Fontannes, F. 1878. Etudes Stratigraphiques et Paléontologiques Pour Servir à l'histoire de La Période Tertiaire Dans Le Bassin Du Rhône. *Soc. Agr., Hist. Nat. Arts utiles. Lyon*, Georg, **4.**

Ford, M., Duchêne, S., Gasquet, D. and Vanderhaeghe, O. 2006. Two-phase orogenic convergence in the external and internal SW Alps. *Journal of the Geological Society*, **163**, 815–826.

Ford, M. and Lickorish, W. H. 2004. Foreland basin evolution around the western Alpine Arc, *Geol. Soc. London, Spec. Publ.*, **221**, 39–63.

Fournier, F., Tassy, A., Thinon, I., Münch, P., Cornée, J.J., Borgomano, J., Leonide, P., Beslier, M.O., Fournillon, A. and Gorini, C. 2016. Pre-Pliocene tectonostratigraphic framework of the Provence continental shelf (eastern Gulf of Lion, SE France). *Bulletin de la Société géologique de France*, **187**, 187–215.

Frouin, M., Sebag, D., Durand, A., Laignel, B., Saliege, J.-F., Mahler, B.J. and Fauchard, C. 2007. Influence of paleotopography, base level and sedimentation rate on estuarine system response to the Holocene sea-level rise: the example of the Marais Vernier, Seine estuary, France. *Sedimentary Geology*, **200**, 15–29.

Garefalakis, P. and Schlunegger, F. 2019. Deciphering tectonic, eustatic and surface controls on the 20 Ma-old Burdigalian transgression recorded in the Upper Marine Molasse in Switzerland. *Solid Earth Discussions*, 1–43, https://doi.org/10.5194/se-2019-27.

Gidon, M., Arnaud, H. and Montjuvent, A. 1978. Notice explicative, Carte géol. France (1/50000), feuille Grenoble (772), *BRGM*, 1-37.

Gigot, P., Colomb, E., Damiani, L., Dubar, L., Durozoy, G. and Thomel, G. 1982. Notice explicative, Carte géol. France (1/50000), feuille de Forcalquier (943). *BRGM*, 1-27.

Gigot P., Grandjacquet C. and Haccard D. 1974. Evolution tectono-sédimentaire de la bordure septentrionale du bassin tertiaire de Digne depuis l'Eocène, *Bull. Soc. Géol. Fr.*, Sér. 7, **16**, 2, 128-139.

Ginsburg, L. and Mongin, D. 1956. Observations nouvelles sur le Miocène de Vence (Alpes-Maritimes). *CR Acad. Sci. Paris*, **242**, 3044.

Ginsburg, L., Arnaud, M., Lary, C. and Monleau, C. 1998. Le Miocène du bassin de Vence (Alpes-Maritimes, France): stratigraphie et paléogéographie. *Geodiversitas*, **20**, 229–238.

Goguel, J. 1936. Description tectonique de la bordure des Alpes de la Bléone au Var. *Mém. Expl. Carte géol. dét. France*, **253**, 367–382.

Grosjean, A., Pittet, B., Gardien, V., Leloup, P., Mahéo, G. and Barraza Garcia, J. 2017. Tectonic heritage in drainage pattern and dynamics: the case of the F rench South Alpine Foreland Basin (ca. 45–20 Ma). *Basin Research*, **29**, 26–50.

Grunert, P., Soliman, A., Ćorić, S., Roetzel, R., Harzhauser, M., and Piller, W.E. (2012). Facies development along the tideinfluenced shelf of the Burdigalian Seaway: An example from the Ottnangian stratotype (Early Miocene, middle Burdigalian). *Marine Micropaleontology*, **84**, 14–36.

Gudefin, H., Donsimoni, M. and Greber, C. 1980. Region de l'Est Lyonnais, Aperçu Géologique d'après Les Forages Profonds. *BRGM*, Report 79, SGN, 596, RHA.

Guérin, C. and Mein, P. 1971. Les principaux gisements de mammifères miocènes et pliocènes du domaine rhodanien. Documents du Laboratoire de Géologie de la Faculté des Sciences de Lyon, 1, 131–170.

Guy, L., Rubino, J.L. and Trémolières, P. 1989. Stratigraphie séquentielle et modalités de comblement des vallées incisées. Le Burdigalien de Montbrun-les- Bains et Chateauneuf-Miravail (SE France). *In*: 2ème Congrès Sedim., Assoc. Sedim. Fr. 147–148.

Haccard, D., Beaudouin, B., Gigot, P. and Jorda, M. 1989. Notice explicative, Carte géologique de France (1/50000), feuille La Javie (918). *BRGM*, 1-152.

Haug, E. 1891. *Les chaînes subalpines entre Gap et Digne: contribution à l'histoire géologique des Alpes françaises*. Ph.D Thesis, Université de Paris.

Herwegh, M., Berger, A., Baumberger, R., Wehrens, P. and Kissling, E. 2017. Large-scale crustal-block-extrusion during late Alpine collision. *Scientific reports*, **7**, 1–10.

Hirn, A. 1980. Le cadre structural profond d'après les profils sismiques. *In*: Autran A. and Dercourt J. (eds) *Evolutions Géologiques de La France: Texte Intégral du Colloque C7, Géologie de France, du 26e CGI*, Mem. BRGM, 107, 34 – 39.

Homewood, P. 1981. Faciès et environnements de dépôt de la Molasse de Fribourg. *Eclogae Geologicae Helvetiae*, **74**, 29–36.

Hudson, J.D. 1975. Carbon isotopes and limestone cement. *Geology*, **3**, 19–22.

Hudson, J.D. 1977. Stable isotopes and limestone lithification. *Journal of the Geological Society*, **133**, 637–660.

Hülscher, J., Fischer, G., Grunert, P., Auer, G. and Bernhardt, A. 2019. Selective recording of tectonic forcings in an Oligocene/Miocene submarine channel system: insights from new age constraints and sediment volumes from the Austrian Northern Alpine Foreland Basin. *Frontiers in Earth Science*, **7**, 302.

Laworsky, G. 1959. Une coquille de Chlamys dans les poudingues de Roquebrune-Cap-Martin (A.M.). *C.R. somm. Soc. Géol. Fr.*, 213–214.

Laworsky, G. and Curti, M. 1960. La faune des poudingues de Roquebrune (A.M.). *C.R. Acad. Sc.*, **251**, 399–400.

Jeannolin, F. 1985. Sédimentologie et hydrogéologie du Néogène de l'Est valentinois et du bassin de Crest (Drôme, France). Ph.D. Thesis, Université Scientifique et Médicale de Grenoble.

Jost, J., Kempf, O. and Kälin, D. 2016. Stratigraphy and palaeoecology of the Upper Marine Molasse (OMM) of the central Swiss Plateau. *Swiss Journal of Geosciences*, **109**, 149–169.

Kalifi, A., Sorrel, P., et al. 2020. Changes in hydrodynamic process dominance (wave, tide or river) in foreland sequences: The subalpine Miocene Molasse revisited (France). *Sedimentology*, **63**, 2455–2501, https://doi.org/10.1111/sed.12708.

Kalifi, A. 2020. *Caractérisation sédimentologique et distribution des dépôts syn-orogéniques Miocènes des chaines subalpines septentrionales (Royans-Vercors-Chartreuse-Bauges), du sud du Jura et du Bas-Dauphiné. Cadre chronostratigraphique et tectonostratigraphique*. Ph.D. Thesis, University of Lyon 1. https://hal.archives-ouvertes.fr/tel-03198092.

Kalifi, A., Leloup, P.H., Sorrel, P., Galy, A., Demory, F., Spina, V., Huet, B., Quillévéré, F., Ricciardi, F., Michoux, D., Lecacheur, K., Grime, R., Pittet, B., and Rubino, J.-L. 2021. Chronology of thrust propagation from an updated tectono-sedimentary framework of the Miocene molasse (western Alps), *Solid Earth*, **12**, 1-37.

Kälin, D. and Kempf, O. 2009. High-resolution stratigraphy from the continental record of the Middle Miocene Northern Alpine Foreland Basin of Switzerland. *Neues Jahrbuch für Geologie und Paläontologie-Abhandlungen*, **254**, 177–235.

Kälin, D. 1997. Litho-und Biostratigraphie der mittel-bis obermiozänen Bois de Raube-Formation (Nordwestschweiz). *Eclogae Geologicae Helvetiae*, **90**, 97–114.

Kempf, O., Matter, A., Burbank, D.W. and Mange, M. 1999. Depositional and structural evolution of a foreland basin margin in a magnetostratigraphic framework: the eastern Swiss Molasse Basin. *International Journal of Earth Sciences*, **88**, 253–275.

Kempf, O. and Matter, A. 1999. Magnetostratigraphy and depositional history of the Upper Freshwater Molasse (OSM) of eastern Switzerland. *Eclogae Geologicae Helvetiae*, **92**, 97–103.

Kempf, O., Bolliger, T., Kälin, D., Engesser, B. and Matter, A. 1997. New magnetostratigraphic calibration of Early to Middle Miocene mammal biozones of the North Alpine foreland basin Aguilar, J.-P., Legendre, S. and Michaux, J. (eds). *Actes du Congrès BiochroM'97. Mémoires et Travaux de l'École pratique de Hautes-Études*, 547–561.

Lamiraux, C. 1977. *Géologie Du Miocène Des Chainons Jurassiens Méridionaux et Du Bas-Dauphiné Nord Oriental Entre Chambéry et La Tour Du Pin: Étude Stratigraphique, Sédimentologique et Tectonique.* Ph.D. Thesis, Université Scientifique et Médicale de Grenoble.

Lapparent, A.F. 1938. Études géologiques dans les régions provençales et alpines entre le Var et la Durance. *Bull. Serv. Carte géol. France*, **XL 198**, 1-301.

Lapparent de A. 1940. Précisions nouvelles au sujet des diapirs de Suzette (Vaucluse) et de Propiac (Drôme), *Bull. Soc. Géol. Fr.*, 5, **10**, 1, p3.

Lapparent de A. 1941. Les phases de plissement tertiaires dans la région du Mont Ventoux, et de la Montagne de Lure, Bull. *Soc. Géol. Fr.*, 5, 11, n°1, 75-85.

Largois, P. 2000. La molasse miocene du bassin de digne (alpes de haute-provence): interpretation paleoecologique des facies marins, PhD Thesis, Caen University.

Latreille, G. 1969. *La Sédimentation Détritique Au Tertiaire Dans Le Bas-Dauphiné et Les Régions Limitrophes*. Ph.D. Thesis, University of Lyon 1.

Lesueur, J.-L. 1991. *Etude sédimentologique et stratigraphique du bassin paléogène d'Apt, Manosque, Forcalquier, Alpes de Haute-Provence, modalités de la transgression burdigalienne.* PhD Thesis, University of Bordeaux.

Lesueur, J.-L., Rubino, J.-L. and Giraudmaillet, M. 1990. Organisation et structures internes des dépôts tidaux du Miocène rhodanien. *Bulletin de la Société géologique de France*, **6**, 49–65.

Lettéron, A., Fournier, F., et al. 2017. Multi-proxy paleoenvironmental reconstruction of saline lake carbonates: Paleoclimatic and paleogeographic implications (Priabonian-Rupelian, Issirac Basin, SE France). *Sedimentary Geology*, **358**, 97–120.

Longhitano, S.G. 2013. A facies-based depositional model for ancient and modern, tectonically–confined tidal straits. *Terra Nova*, **25**, 446–452.

Longhitano, S.G., Chiarella, D. and Muto, F. 2014. Three-dimensional to two-dimensional cross-strata transition in the lower Pleistocene Catanzaro tidal strait transgressive succession (southern Italy). *Sedimentology*, **61**, 2136–2171, https://doi.org/10.1111/sed.12138.

Lopez, S., Cojan, I. and Renard, M. 2000. Corrélations chimiostratigraphiques entre domaines marin et continental : application à une série du Miocène inférieur (Beynes-Châteauredon, Alpes-de-Haute-Provence, France). *Comptes Rendus de l'Académie des Sciences-Series IIA-Earth and Planetary Science*, **330**, 837–843.

Malikides, M., Harris, P.T., Jenkins, C.J. and Keene, J.B. 1988. Carbonate sandwaves in Bass Strait. *Australian Journal of Earth Sciences*, **35**, 303–311.

Maridet, O. 2002. Proposition of dating a Miocene Alpine tectonic event using mammal biochronology: example of the Four karst filling. *Geodinamica Acta*, **15**, 179–184.

Maridet, O. 2003. *Révision Du Genre Democricetodon (Mammalia, Rodentia, Cricetinae) et Dynamique Des Faunes de Rongeurs Du Néogène d'Europe Occidentale : Évolution, Paléobiodiversité et Paléobiogéographie*. Ph.D Thesis, University of Lyon I.

Maridet, O., Berthet, D. and Mein, P. 2000. Un nouveau gisement karstique polyphasé miocène moyen de Four (Isère): étude des Cricetidae (Mammalia, Rodentia) et description de Semocricetodon fourensis nov. sp. *Géologie de la France*, **2**, 71–79.

Mascle, A., Vially, R., Deville, E., Biju-Duval, B. and Roy, J.P. 1996. The petroleum evaluation of a tectonically complex area: the western margin of the Southeast Basin (France). *Marine and Petroleum Geology*, **13**, 941–961.

McArthur, J.M., Howarth, R.J. and Shields, G.A. 2012. Strontium isotope stratigraphy. *In*: Gradstein, F. M., Ogg, J. G., Schmitz, M. D., & Ogg, G. M. (eds), *The geologic time scale*, Elsevier, **1**, 127–144.

Meckel, L.D. 1997. *Sedimentological and structural evolution of the Tertiary Dévoluy Basin, external western Alps, SE France*. Ph.D. Thesis, ETH Zurich.

Meckel, L.D., Ford, M. and Bernoulli, D. 1996. Tectonic and Sedimentary Evolution of the Dévoluy Basin, a Remnant of the Tertiary Western Alpine Foreland Basin, SE France. *Géologie de la France*, 2, 2-26.

Mein, P. and Ginsburg, L. 2002. Sur l'âge relatif des différents dépôts karstiques miocènes de La Grive-Saint-Alban (Isère). *Publications du musée des Confluences*, **5**, 7–47.

Mein, P., Truc, G. and Demarcq, G. 1971. Micromammifères et gastéropodes continentaux des biozones de Paulhiac et de La romieu dans le Miocène de La Bastidonne et de Mirabeau (Vaucluse, SE de la France). *CR Acad. sci.*, **273**, 566–568.

Menard, G. and Thouvenot, F. 1987. Balanced cross-sections at crustal scale-methods and application to the western Alps. *Geodin. Acta*, **1**, 35–45.

Meulenkamp, J.E. and Sissingh, W. 2003. Tertiary palaeogeography and tectonostratigraphic evolution of the Northern and Southern Peri-Tethys platforms and the intermediate domains of the African–Eurasian convergent plate boundary zone. *Palaeogeography, Palaeoclimatology, Palaeoecology*, **196**, 209–228.

Miller, K.G., Kominz, M.A., et al. 2005. The phanerozoic record of global sea-level change. *Science*, **310**, 1293–1298, https://doi.org/10.1126/science.1116412.

Mongin, D. 1949. Sur la présence du Burdigalien moyen dans la région de Fontvieille (Bouches-du-Rhône). *C. R. Somm. Soc. Géol Fr*, 292.

Mongin, D. 1962. Au sujet des pectinidés du Miocène de Vence (Alpes-Maritimes). *Comptes Rendus sommaires de la Société géologique de France*, **1**, 24–25.

Montenat, C., Barrier, P. and Garnier, L. 2000. La sédimentation miocène au nord des massifs de Ventoux-Lure (chaînes subalpines méridionales). *Géologie de la France*, **3**, 3–32.

Mugnier, J.L., Guellec, S., Menard, G., Roure, F., and Tardy, M. 1990. A crustal scale balanced cross-section through the external Alps deduced from the ECORS profile. *Mémoires la Société géologique Fr.*, **156**, 203–216.

Mugnier, J., Arpin, R., and Thouvenot, F. 1987. Balanced cross-sections through the subalpine massif of the Chartreuse. *Geodin. Acta*, **1**, 125–137.

Nelson, C.S. and Smith, A.M. 1996. Stable oxygen and carbon isotope compositional fields for skeletal and diagenetic components in New Zealand Cenozoic nontropical carbonate sediments and limestones: a synthesis and review. *New Zealand Journal of Geology and Geophysics*, **39**, 93–107.

Nicolet, C. 1979. *Le Bas-Dauphiné Septentrional : Étude Stratigraphique et Sédimentologique*. Ph.D. Thesis, Université Scientifique et Médicale de Grenoble.

Odebode, M.O. 1978. The Age of the Marly Formation of the Miocene Basin of Vence (SE France) based on Planktonic Foraminifera. *Revista espanola de micropaleontologia*, **10**, 75–86.

Odebode, M.O. 1982. Miocene foraminiferal paleoecology of the basin of Vence, Southeast France. *Palaeogeography, Palaeoclimatology, Palaeoecology*, **39**, 313–329.

Ogg, J.G., Ogg, G.M. and Gradstein, F.M. 2016. A Concise Geologic Time Scale: 2016, Elsevier.

Olariu, C., Steel, R.J., Dalrymple, R.W. and Gingras, M.K. 2012. Tidal dunes versus tidal bars: The sedimentological and architectural characteristics of compound dunes in a tidal seaway, the lower Baronia Sandstone (Lower Eocene), Ager Basin, Spain. *Sedimentary Geology*, **279**, 134–155.

Oudet, J., Münch, P., Borgomano, J. Quillevere, F., Melinte-Dobrinescu, M.C., Demory, F., Viseur, S. and Cornee, J.J. 2010. Land and sea study of the northeastern golfe du Lion rifted margin: the Oligocene–Miocene of southern Provence (Nerthe area, SE France). *Bulletin de la Société géologique de France*, **181**, 591–607, https://doi.org/10.2113/gssgfbull.181.6.591

Pfiffner, O.A. 1986. Evolution of the north Alpine foreland basin in the Central Alps. In: Allen, P. A. and Homewood, P. (eds) *Foreland Basins*. 219–228.

Philippe, Y., Colletta, B., Deville, E. and Mascle, A. 1996. The Jura fold-and-thrust belt: a kinematic model based on map-balancing. *Mémoires du Muséum national d'histoire naturelle*, **170**, 235–261.

Philippe, Y., Deville, E. and Mascle, A. 1998. Thin-skinned inversion tectonics at oblique basin margins: example of the western Vercors and Chartreuse Subalpine massifs (SE France). *Geological Society, London, Special Publications*, **134**, 239–262.

Picot, L., Becker, D., Cavin, L., Pirkenseer, C., Lapaire, F., Rauber, G., Hochuli, P.A., Spezzaferri, S. and Berger, J.P. 2008. Sédimentologie et paléontologie des paléoenvironnements côtiers rupéliens de la Molasse marine rhénane dans le Jura suisse. *Swiss Journal of Geosciences*, **101**, 483–513.

Pippèrr, M. and Reichenbacher, B. 2017. Late Early Miocene palaeoenvironmental changes in the North Alpine Foreland Basin. *Palaeogeography, Palaeoclimatology, Palaeoecology*, **468**, 485–502.

Posamentier, H.W. and Allen, G.P. 1999. Siliciclastic sequence stratigraphy: concepts and applications. *SEPM (Society for Sedimentary Geology) Tulsa*, Oklahoma, **7**, https://doi.org/10.2110/csp.99.07

Prodehl, C. and Haak, V. 2006. The European cenozoic rift system. *In*: Olsen, K.H. (ed) *Developments in Geotectonics: Continental rifts: evolution, structure, tectonics*. Elsevier, 25, 133–212.

Pugh, D. 1987. *Tides, Surges and Mean Sea-Level: a handbook for engineers and scientists*. John Wiley and Sons, New-York.

Reynaud, J.Y. and Dalrymple, R.W. 2012. Shallow-marine tidal deposits. *In:* Davis, R. A. and Dalrymple, R. W. (eds) *Principles of Tidal Sedimentology*. Springer, 335–369.

Reynaud, J.-Y., Vennin, E., Parize, O., Rubino, J.-L. and Bourdillon, C. 2012. Incised valleys and tidal seaways: the example of the Miocene Uzès-Castillon basin, SE France. *Bulletin de la Société Géologique de France*, **183**, 471–486.

Reynaud, J.-Y., Ferrandini, M., et al. 2013. From non-tidal shelf to tide-dominated strait: The Miocene Bonifacio Basin, Southern Corsica. *Sedimentology*, **60**, 599–623.

Ricketts, B.D. and Evenchick, C.A. 2007. Evidence of different contractional styles along foredeep margins provided by Gilbert deltas: examples from Bowser Basin, British Columbia, Canada. *Bulletin of Canadian Petroleum Geology*, **55**, 243–261.

Rossi, V.M., Longhitano, S.G., Mellere, D., Dalrymple, R.W., Steel, R.J., Chiarella, D. and Olariu, C. 2017. Interplay of tidal and fluvial processes in an early Pleistocene, delta-fed, strait margin (Calabria, Southern Italy). *Marine and Petroleum Geology*, **87**, 14–30, https://doi.org/10.1016/j.marpetgeo.2017.02.021.

Roussé, S., Filleaudeau, P.-Y., Mermy, G.C., Letteron, A. and Schaming, M. 2016. Integrated stratigraphic and petroleum system modeling study of the southern upper Rhine Graben. In: *AAPG/SEG International Conference and Exhibition*. 3rd-6th April, Barcelona, Spain.

Rubino, J.L., Lesueur, J.L. and Clauzon, G. 1990. *Le Miocène Inférieur et Moyen Du Bassin Rhodanien: Stratigraphie Séquentielle et Sédimentologie*, Field Trip Guidebook: Special Publication of the Association des Sédimentologistes Français.

Rubino, J.L., Bez, M., Crumeyrolle, P., Largois, P., Parize, O. and Besson, D. 2015. La Molasse Miocène du bassin de Digne : Révision stratigraphique et paléogéographique. In: *15^{e} congrès français de sédimentologie*, ASF, 13-15 October, Chambéry, France.

Rubino, J.L., Kalifi, A., et al. 2019. Spatial evolution of depositional processes in the Aquitanian alpine Gulf in SE France, a precursor of Burdigalian peri alpine seaway. In: *34th IAS meeting of sedimentology*. IAS, 10-13 September, Roma, Italia.

Sant, K., V. Palcu, D., Mandic, O. and Krijgsman, W. 2017. Changing seas in the Early–Middle Miocene of Central Europe: a Mediterranean approach to Paratethyan stratigraphy. *Terra Nova*, **29**, 273–281.

Schlunegger, F., Burbank, D.W., Matter, A., Engesser, B. and Mödden, C. 1996. Magnetostratigraphic calibration of the Oligocene to Middle Miocene (30-15 Ma) mammal biozones and depositional sequences of the Swiss Molasse Basin. *Eclogae Geologicae Helvetiae*, **89**, 753–788.

Schlunegger, F., Leu, W. and Matter, A. 1997. Sedimentary sequences, seismic facies, subsidence analysis, and evolution of the Burdigalian Upper Marine Molasse Group, central Switzerland. *AAPG bulletin*, **81**, 1185–1207.

Sinclair, H.D. and Allen, P.A. 1992. Vertical versus horizontal motions in the Alpine orogenic wedge: Stratigraphic response in the foreland basin. *Basin Research*, **4**, 215–232, https://doi.org/10.1111/j.1365-2117.1992.tb00046.x.

Sissingh, W. 2001. Tectonostratigraphy of the West Alpine Foreland: correlation of Tertiary sedimentary sequences, changes in eustatic sea-level and stress regimes. *Tectonophysics*, **333**, 361–400.

Sissingh, W. 2003. Tertiary paleogeographic and tectonostratigraphic evolution of the Rhenish Triple Junction. *Palaeogeography, Palaeoclimatology, Palaeoecology*, **196**, 229–263.

Smeraglia, L., Looser, N., Fabbri, O., Choulet, F., Guillong, M. and Bernasconi, S.M. 2021. U-Pb dating of middle Eocene-middle Pleistocene multiple tectonic pulses in the Alpine foreland. *Solid Earth Discussions*, [preprint], 1–14.

Steininger, F.F., Berggren, W.A., Kent, D.V., Bernor, R.L., Sen, S. and Agusti, J. 1996. Circum-Mediterranean Neogene (Miocene and Pliocene) marine-continental chronologic correlations of European mammal units. *In*: Bernor, R.L., Fahlbusch, V. and Mittmann, H. W. (eds) *The Evolution of Western Eurasian Neogene Mammal Faunas*, Columbia Univ. Press, New York, 7-46.

Strunck, P., and Matter, A. (2002). Depositional evolution of the western Swiss Molasse. *Eclogae Geologicae Helvetiae*, **95**, 197-222.

Thome, M., Rubino, J.L., Clauzon, G. and Lesueur, J.L. 1989. Identification des limites de séquences de dépôts en système fluviatile: le cas du Miocène de Châteauredon (SE France). *Mém. ASF, Paris*, **2**, 281–282.

Villegier M. 1984. Evolution du Panneau de couverture Nord provençal (Mont Ventoux, Lubéron, Moyenne Durance), PhD Thesis, Univ. Paris sud Orsay, 200p.

Villeger, M. and Andrieux, J. 1987. Phases tectoniques post-Eocènes et structuration polyphasée du panneau de couverture nord provençal (Alpes externes méridionales), *Bulletin de la Société géologique de France*, **3**(1), 147-156.

Von Hagke, C., Cederbom, C.E., Oncken, O., Stöckli, D.F., Rahn, M.K. and Schlunegger, F. 2012. Linking the northern Alps with their foreland: The latest exhumation history resolved by low-temperature thermochronology. *Tectonics*, **31**, TC5010, doi:10.1029/2011TC003078

Ziegler, P.A. 1988. Evolution of the Arctic-North Atlantic and the Western Tethys: A visual presentation of a series of Paleogeographic-Paleotectonic maps. *AAPG memoir*, **43**, 164–196.

Ziegler, P.A. 1990. *Geological atlas of western and central Europe*. Shell Internationale Petroleum Maatschappij Bv and Geological Society Publishing House.

Ziegler, P.A. 1994. Cenozoic rift system of Western and Central-Europe-an overview. *Geologie en Mijnbouw*, **73**, 99–127.

Ziegler, P.A. and Dèzes, P. 2007. Cenozoic uplift of Variscan Massifs in the Alpine foreland: Timing and controlling mechanisms. *Global and Planetary change*, **58**, 237–269.

Figure Captions

Fig. 1: (A) Location map of the peripheral foreland basin of the Cenozoic Alpine orogeny in light green (map from Google Earth); the study area is shown with a red square.NAFB= North Alpine foreland basin; RPMB= Rhodano-Provencal Molasse basin; SMB= Swiss Molasse basin. (B) Location of the Miocene basins (La Bresse, Bas-Dauphiné, Crest basins) of the subalpine massifs (Vercors, Chartreuse, Bauges, Bornes), the southern Jura and the adjacent basins (Bas-Dauphiné, La Bresse, Crest). The main faults are highlighted in orange and labelled 1 to 5, corresponding to Fault Zones (FZ) as defined in Kalifi (2020); Pt=Penninic thrust; GF= Gros Foug thrust; SAL = Saleve thrust; J= Jura thrust. (C) Cross-section throughout the central Chartreuse and Belledonne massif (Kalifi et al. 2021), as localised in Fig. 1B with a dashed red line. BBt= Belledonne basal thrust.

Fig. 2: Summary of the structural, chronostratigraphic and tectonostratigraphic framework (Kalifi et al. 2021) of the study area. (A) Synthetic section of Miocene deposits in the study area and the 11 Miocene depositional sequences; (B) Miller *et al.* (2005) eustatic curve recalibrated to Ogg *et al.* (2016) geochronology. (C) The 12 Miocene palaeogeographical zones grouped into four palaeogeographical domains reveal a clear spatial relation with the five fault zones (FZ1-5). (D) The three alpine compressive phases impacting the Miocene palaeogeography. The main phase (phase P2) involved the progressive onset, from east to west, of the SAL fault, the GF fault, FZ2, FZ3, FZ and FZ5 in response to the onset of the Belledonne basal thrust.

Fig. 3: Oligocene isopach map of the Bas-Dauphiné and Crest basins, Vercors, Chartreuse and southern Jura synclines.

Fig. 4: Palaeogeographic map of the upper Aquitanien S1a sequence and the lower Burdigalian S1b sequence.

Fig. 5: Palaeogeographic maps of the upper Burdigalian S2a (A) and S2b (B) sequences. Fig. 4 for legend.

Fig. 6: Palaeogeographical maps of the late Burdigalian to lower Langhian S3 sequence (A) and the upper Langhian S4 sequence (B). Legend in Fig. 4.

Fig. 7: 3D model of the stacked gilbert-deltas of the Pont Demay cliffs. Red squares = Sedimentological sections, see Fig.1 for map location. Orange circles= Fault zones (FZ). GD= Gilbert delta. Satellite view (A) and the view from the south (B) of the Pont Demay cliffs in the FZ2 footwall. (C) The Pisserotte section is allowing to calibrate the chronostratigraphy of the Pont Demay GDs, belonging to the S4 (GD1) and S5(GD2) sequences. (D) Detailed spatial disposition of the northern and southern Pont Demay cliffs. (E) The S4 sequence in the southern Pont Demay cliff (see F, for the orthogonal section) characterized by two northward prograding GDs (GD1a et GD1b), overlain by sub-horizontal topsets. (F) Orthogonal view of the GDs recorded during S4, in the southern Pont Demay cliff. Curved red arrow= growth-strata. (G, H) The S5 sequence in the northern Pont Demay cliff, characterized by a northward prograding GD (GD2), overlain by ~50m of planar stratified topsets. Close-up view on ~10m high cross-beds with interstratifications of reddish fine-grained deposits that were interpreted as being time-equivalent with those recorded at the base of the S5 sequence of the La Roize section (22, Kalifi, 2020) dated to 12.6-13.6 Ma by combining nannoplankton and mammal (i.e., biostratigraphical) dating.

Fig. 8: Palaeogeographical maps of the late Langhian-lower Serravallian S5a-S5b sequences (A), the upper Serravallian S6 sequence (B), the lower Tortonian S7 sequence (C) and the upper Tortonian S8 sequence (D). Fig. 4 for legend.

Fig. 9: The Western Alpine foreland basin, from the Rhodano-Provencal molasse basin (RPMB) to the Swiss Molasse basin. The RPMB is presented with its different sub-basins (Valréas, Basse-Provence, Apt-Forcalquier, Digne basins) and the localites quoted in the main text.

Fig. 10: The lower Miocene stratigraphy of the Valréas basin. (A) The St-Restitut S1c deposits, filling up an incised palaeovalley (Lesueur *et al.*, 1990; Rubino *et al.* 1990). (B) The Nyons sedimentological section modified from Rubino *et al.* (1990).

Fig. 11: The lower Miocene Miocene seaway palaeogeographical evolution at the scale of the Western Alpine foreland basin. (A) The S1a sequence, between ~21.0 to ~20.6 Ma, (B) The S1b sequence, between ~20.6 to ~17.8 Ma. (C) The S1c sequence, between ~19.8 to ~17.8 Ma, (D) The S2a-S2b sequences, between ~17.8 and ~16.2 Ma, (E) The S3 sequence, between ~16.2 to ~15.0 Ma, (F) The S4-S5a-S5b sequences, between ~15.0 to ~12.0 Ma, (G) The S6-S7 sequences, between ~12.0 to ~9.5 Ma, (H) The S8 sequence, between ~9.5 to ~8.0(?) Ma.

Table Caption

Table 1: $^{87}Sr/^{86}Sr$ dating and $\delta^{18}O$ and $\delta^{13}C$ analyses. The ages and the associated uncertainties appear in bold red characters, and are exploited during the study.

Locality	GPS	$^{87}Sr/^{86}Sr$	±	±	Mean Age	%CaCO3	$\delta^{13}C_{V-PDB}$	±	$\delta^{18}O_{V-PDB}$	±
16 : St-Restitut	44.315571°; 4.787133°	0.708574	0.000016	**0.20**	**17.95**	97.74	-2.44	0.01	-4.81	0.02
		0.708539	0.000016	**0.20**	**18.35**	99.75	-0.80	0.02	-2.44	0.01
		0.708516	0.000021	**0.27**	**18.63**	99.63	-1.16	0.01	-2.50	0.02
15: Nyons	44.359330°; 5.144833°	0.708603	0.000018	**0.20**	**17.60**	97.9	0.69	0.03	-0.84	0.05
	44.416401°; 5.067419°	0.708496	0.000024	**0.32**	**18.88**	100.33	-0.82	0.01	-2.72	0.02

Table 1

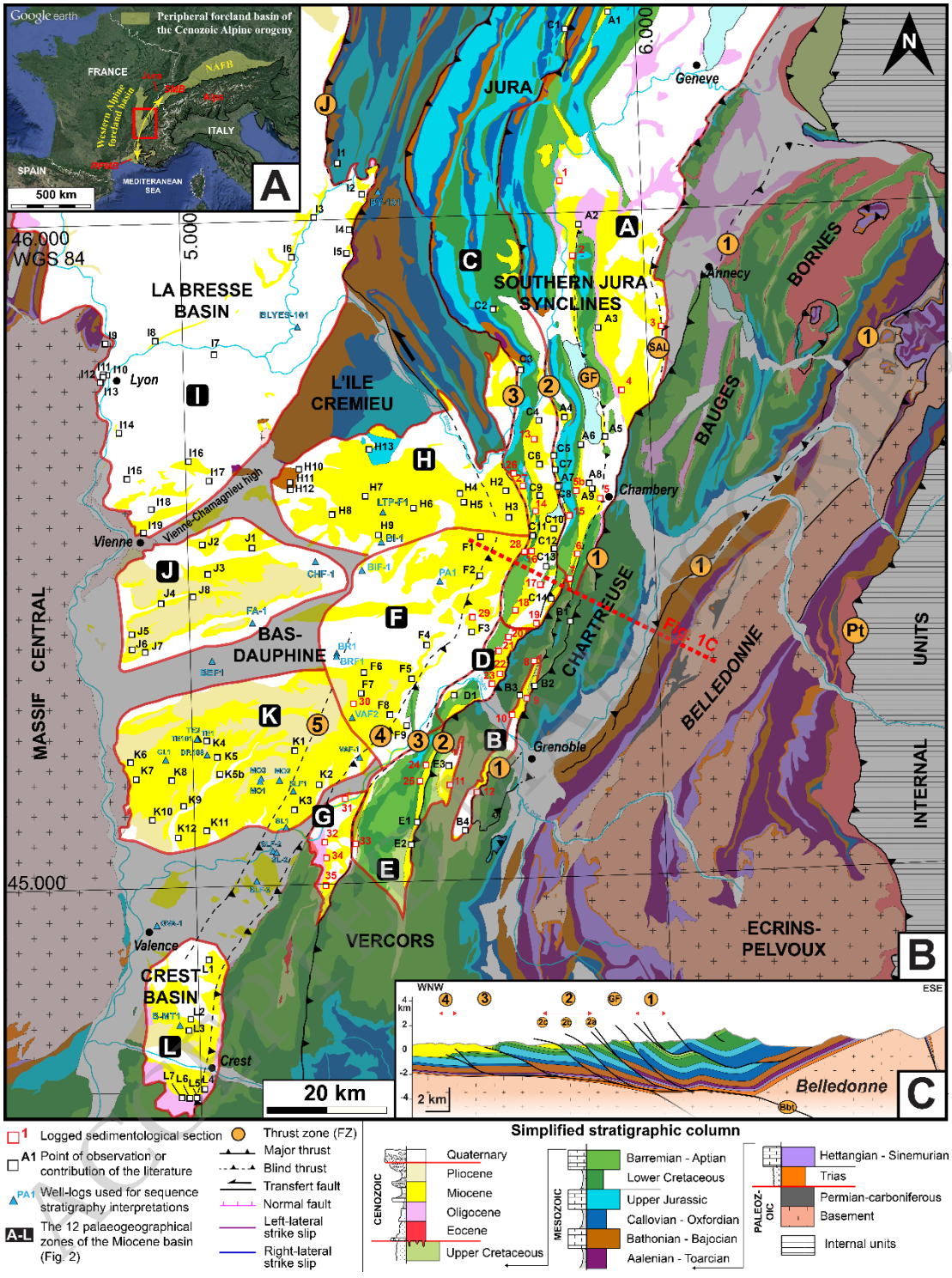

Figure 1

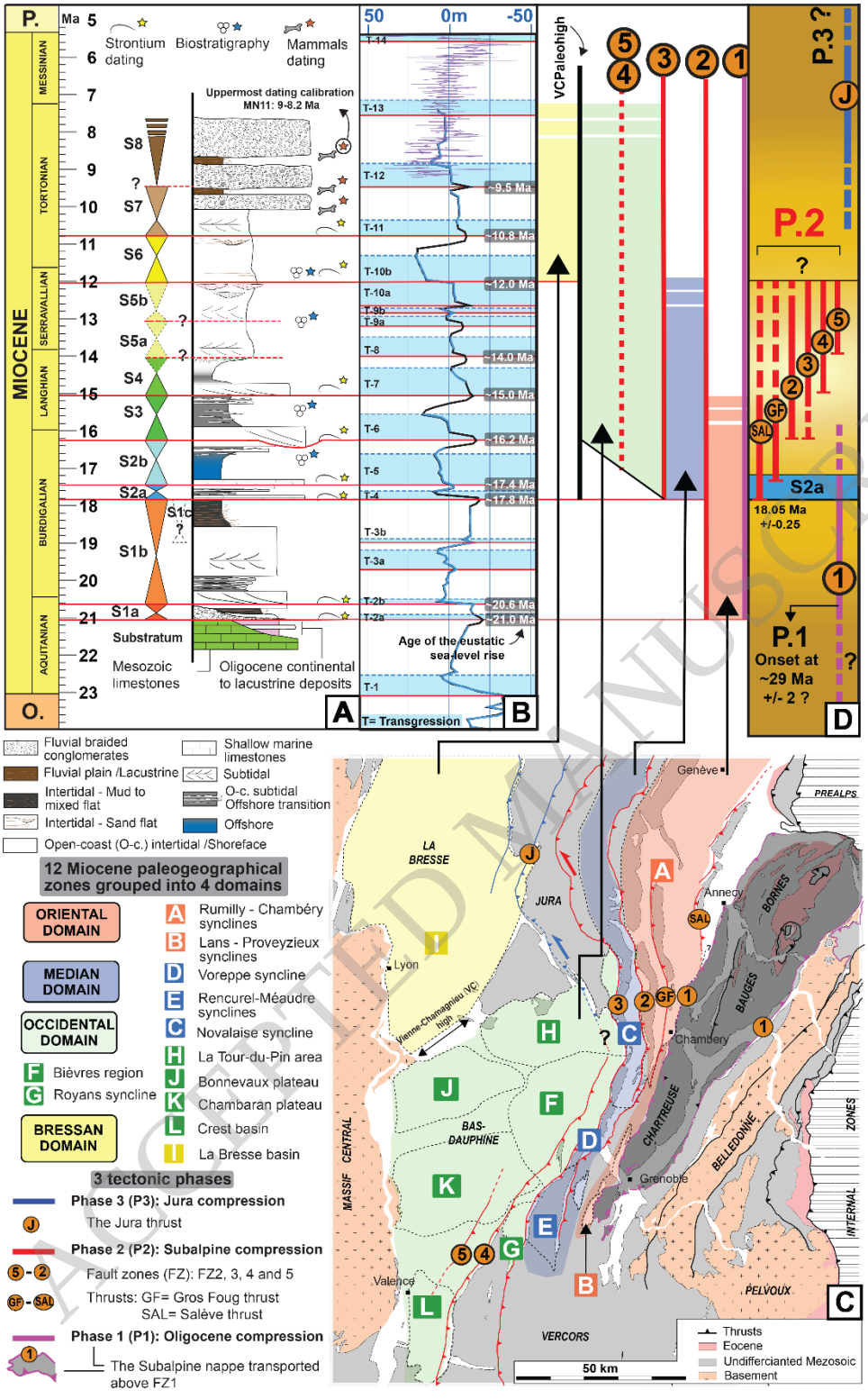

Figure 2

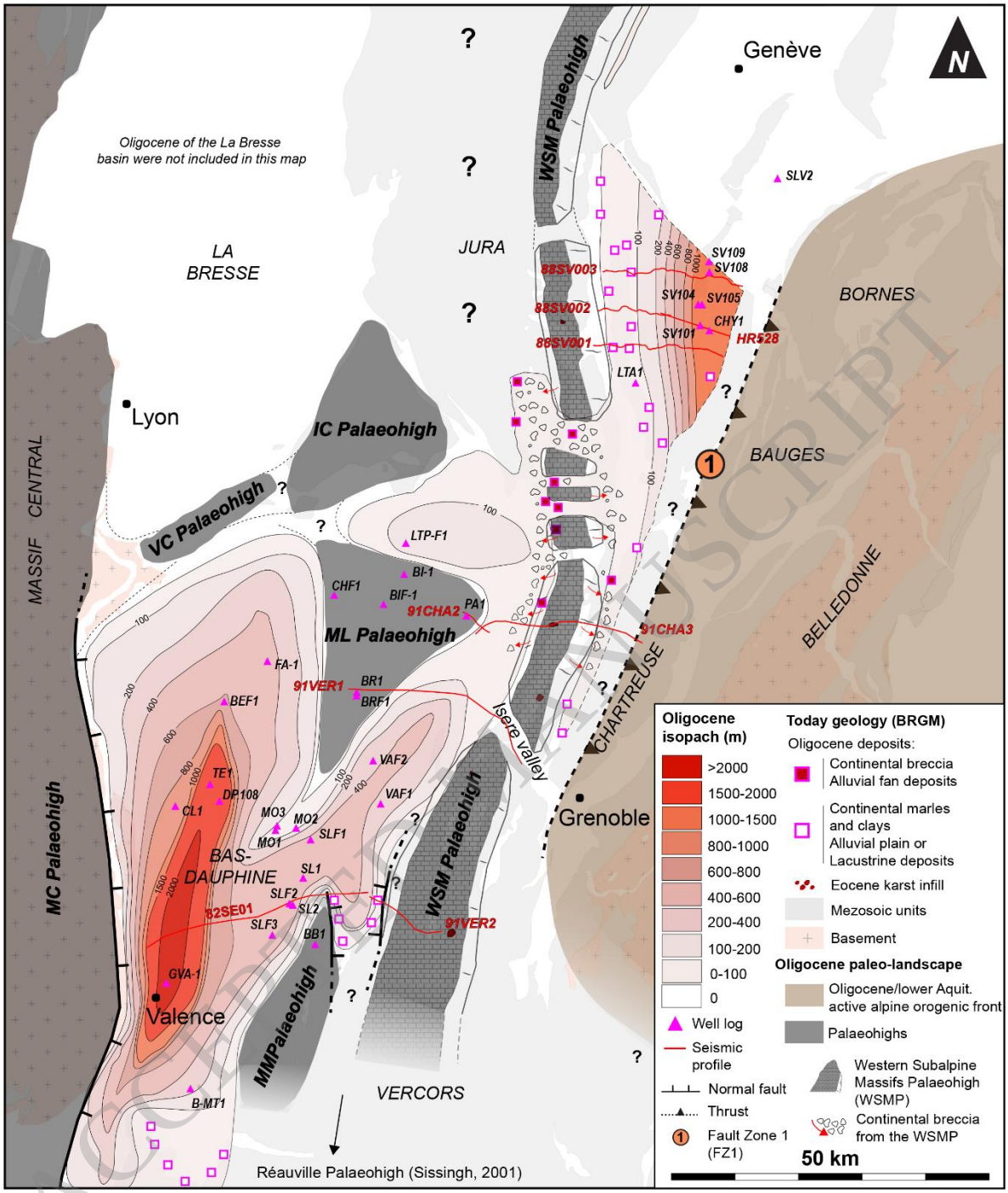

Figure 3

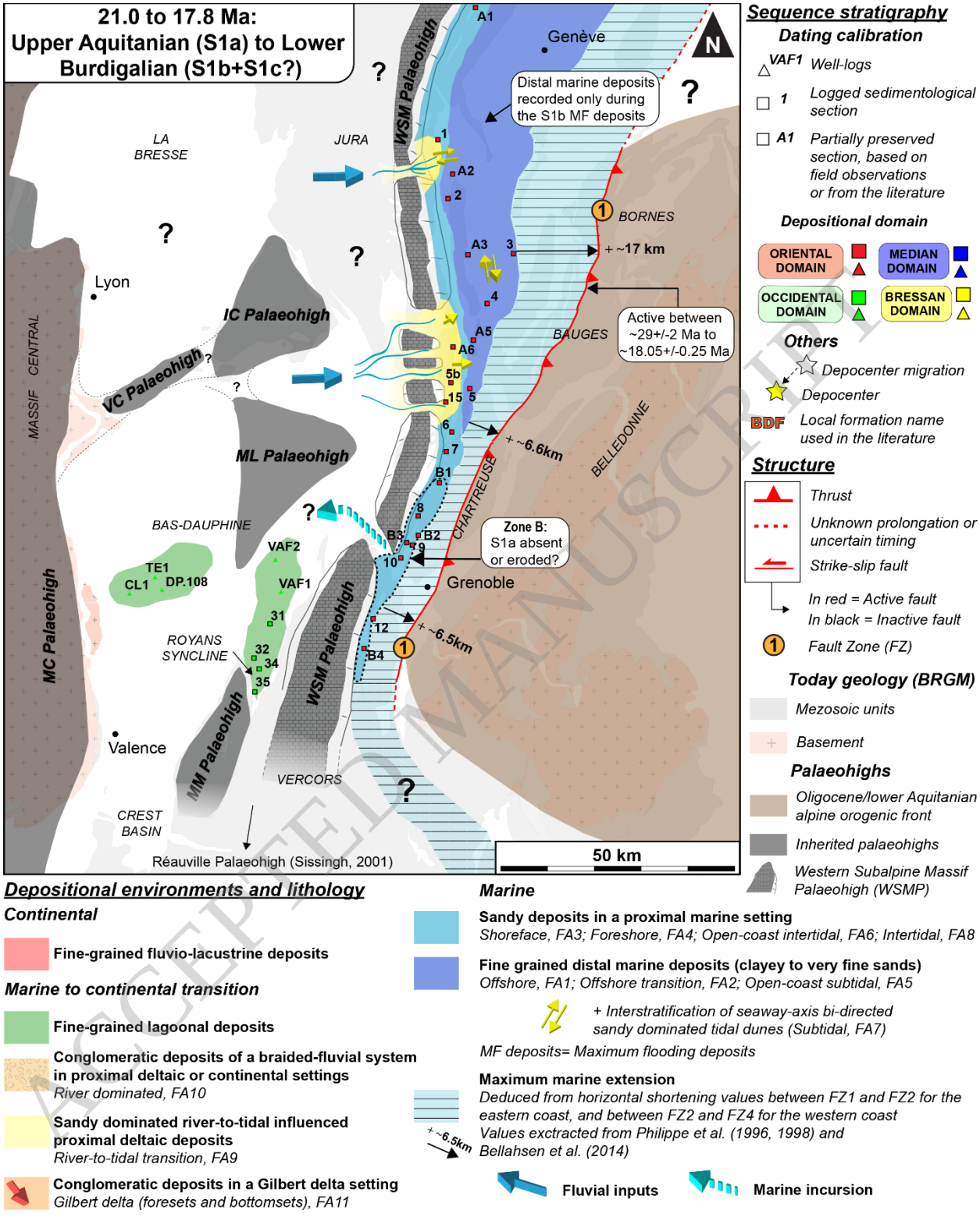

Figure 4

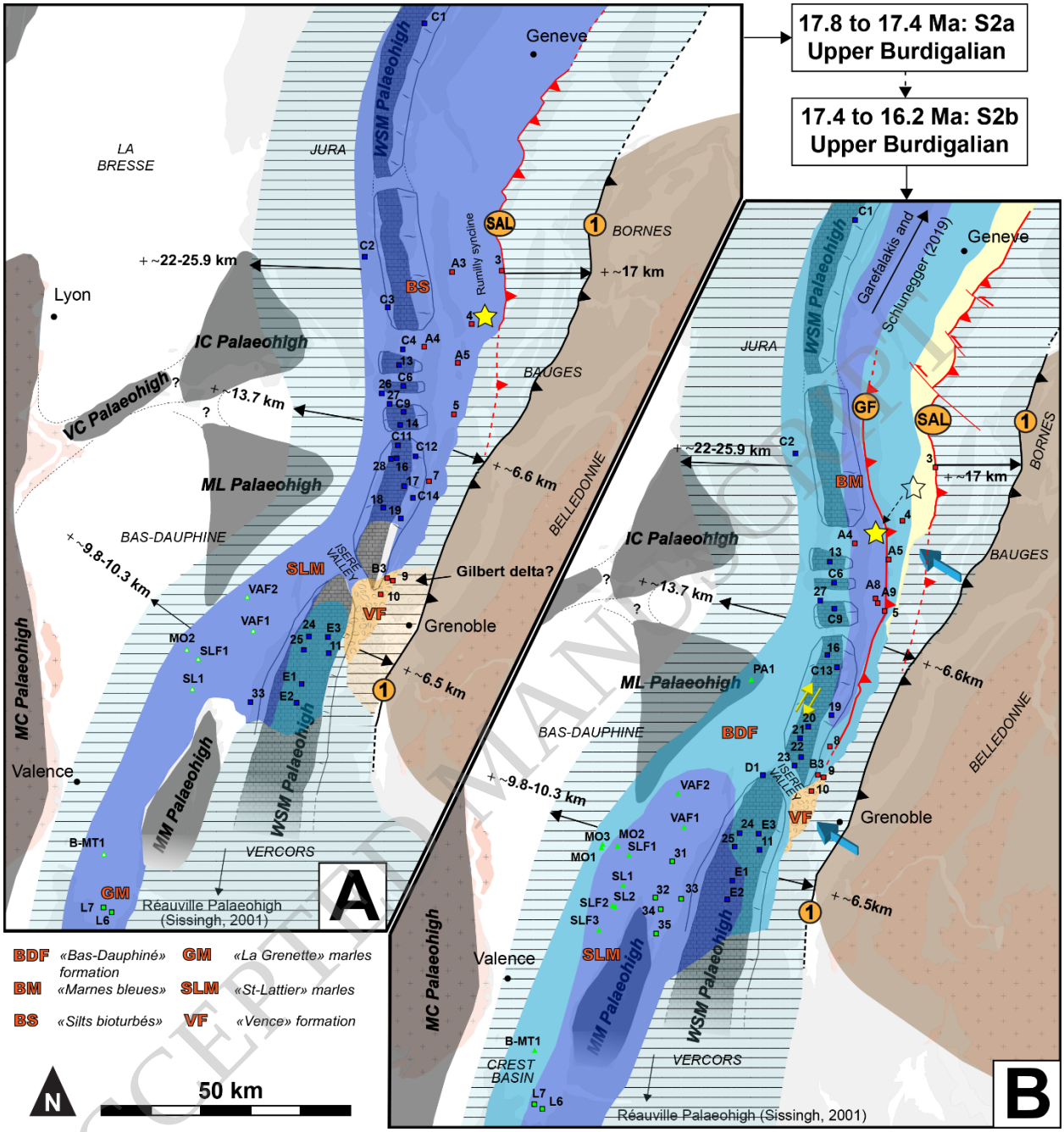

Figure 5

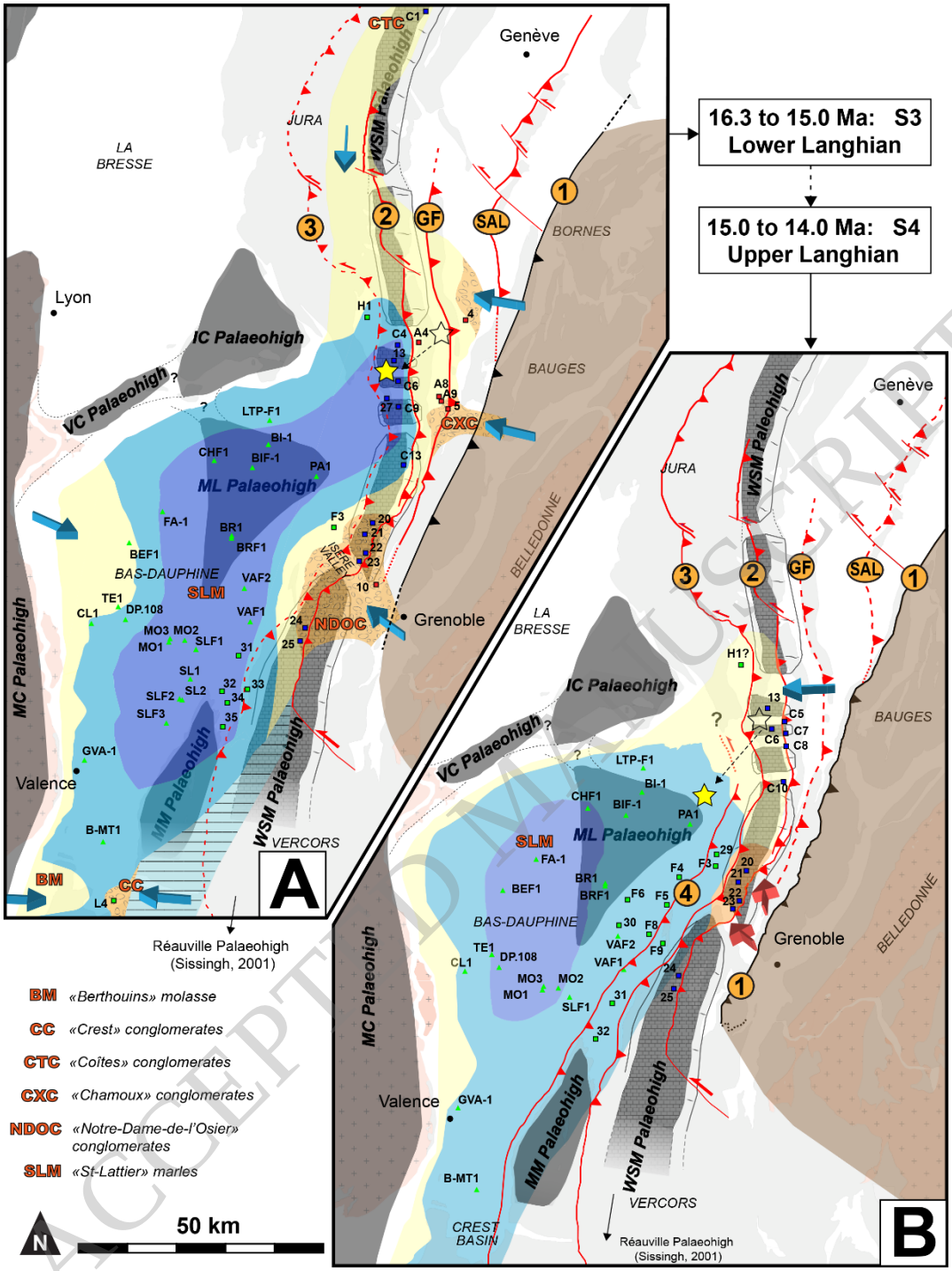

Figure 6

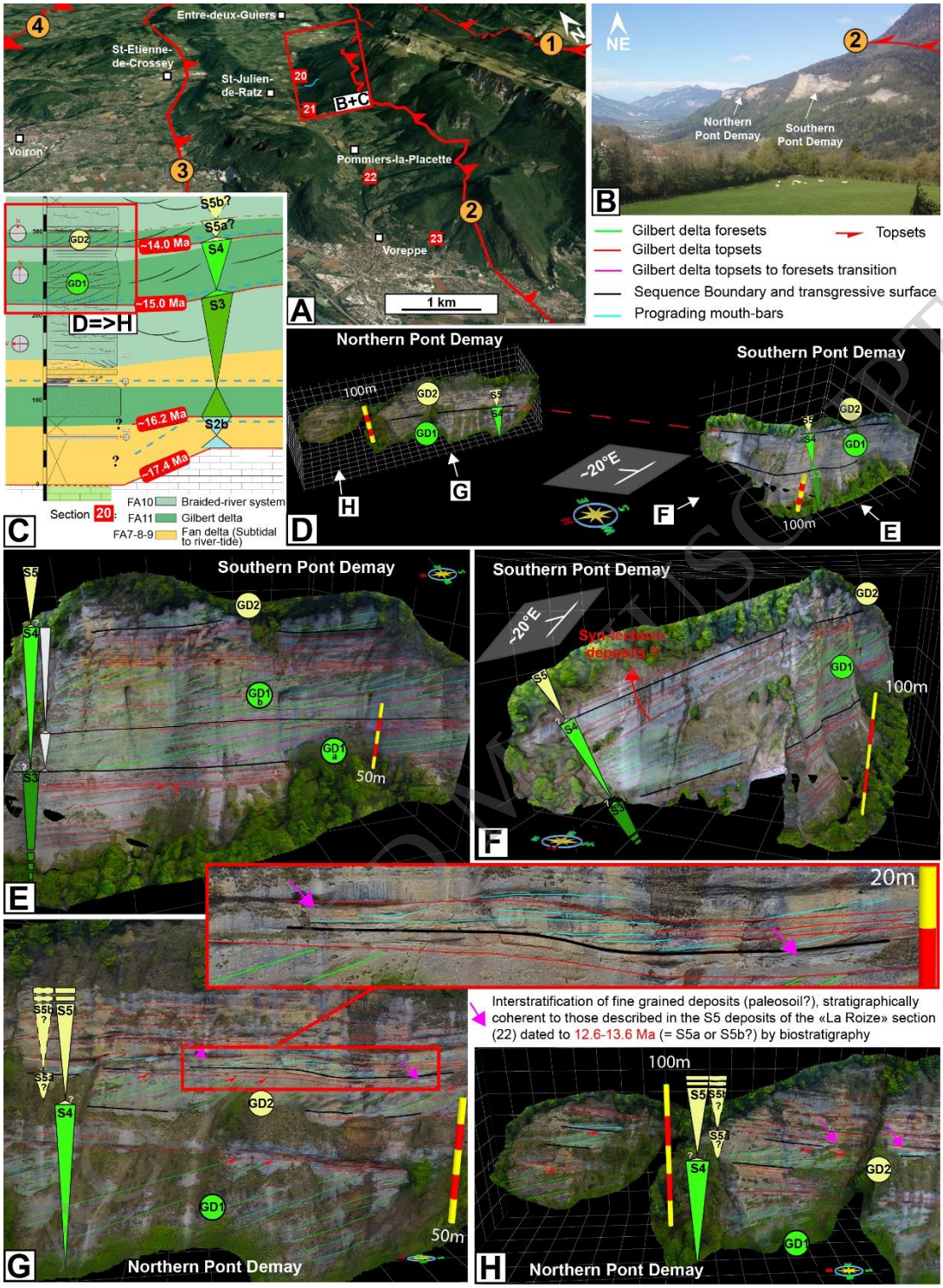

Figure 7

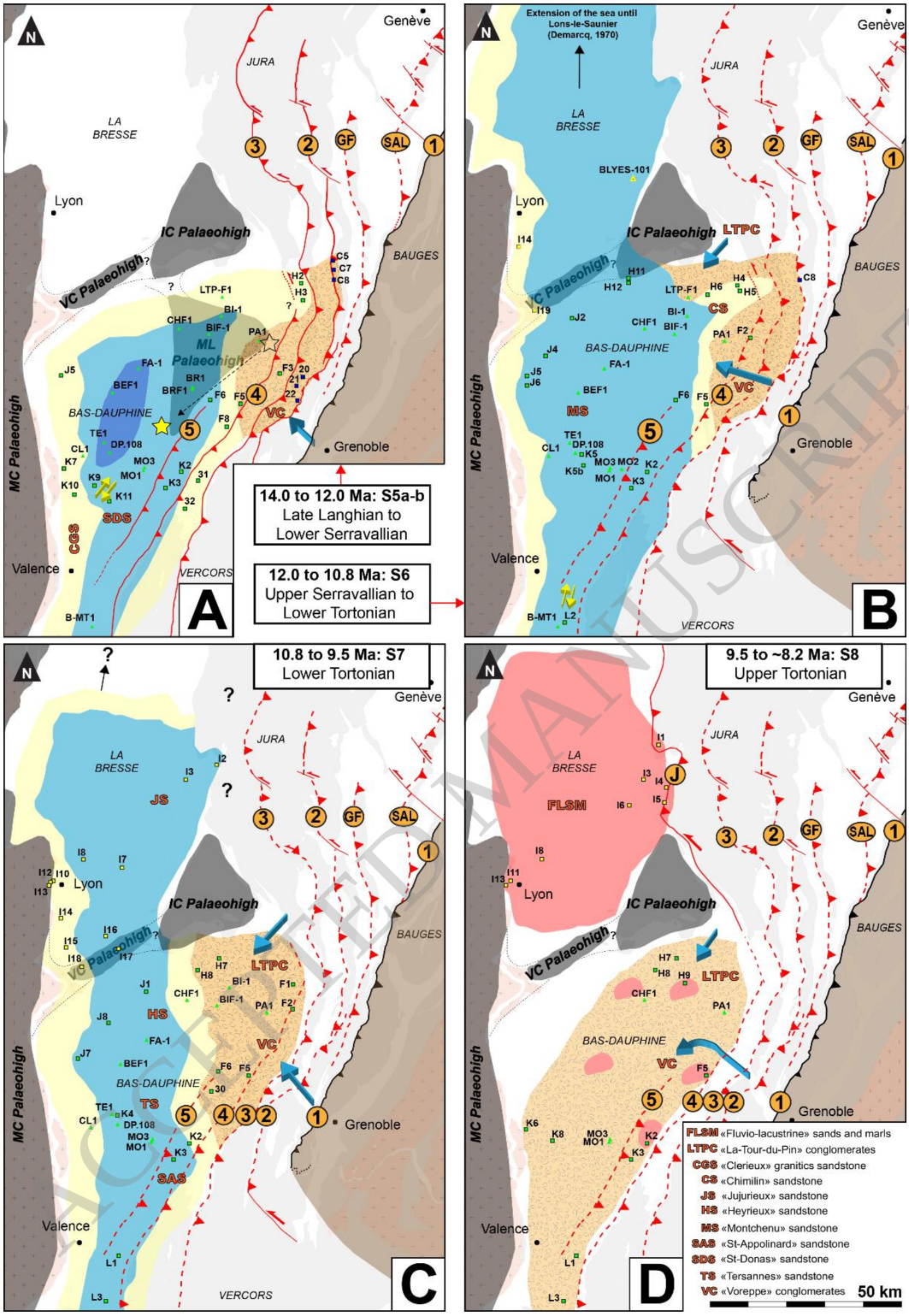

Figure 8

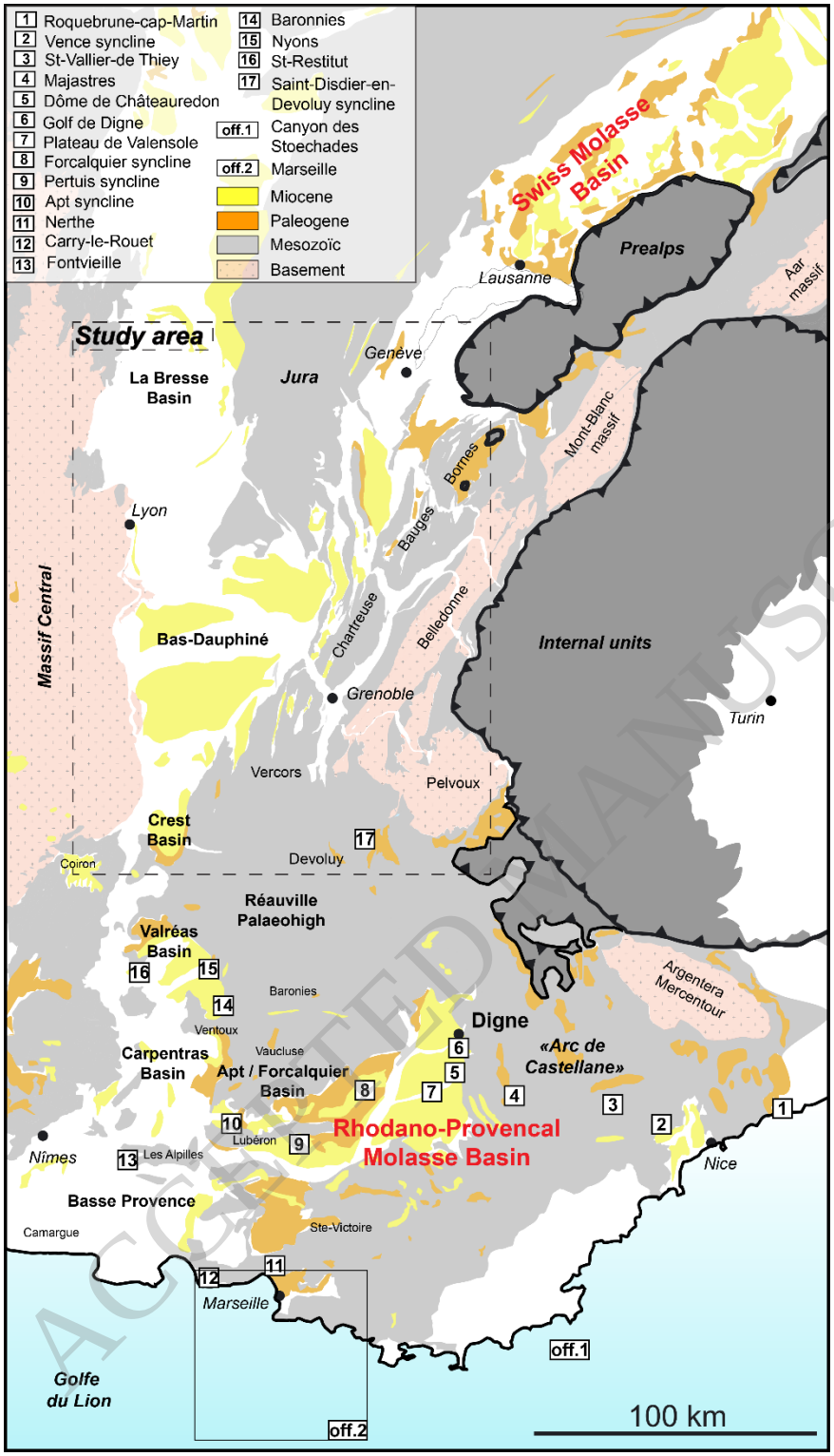

Figure 9

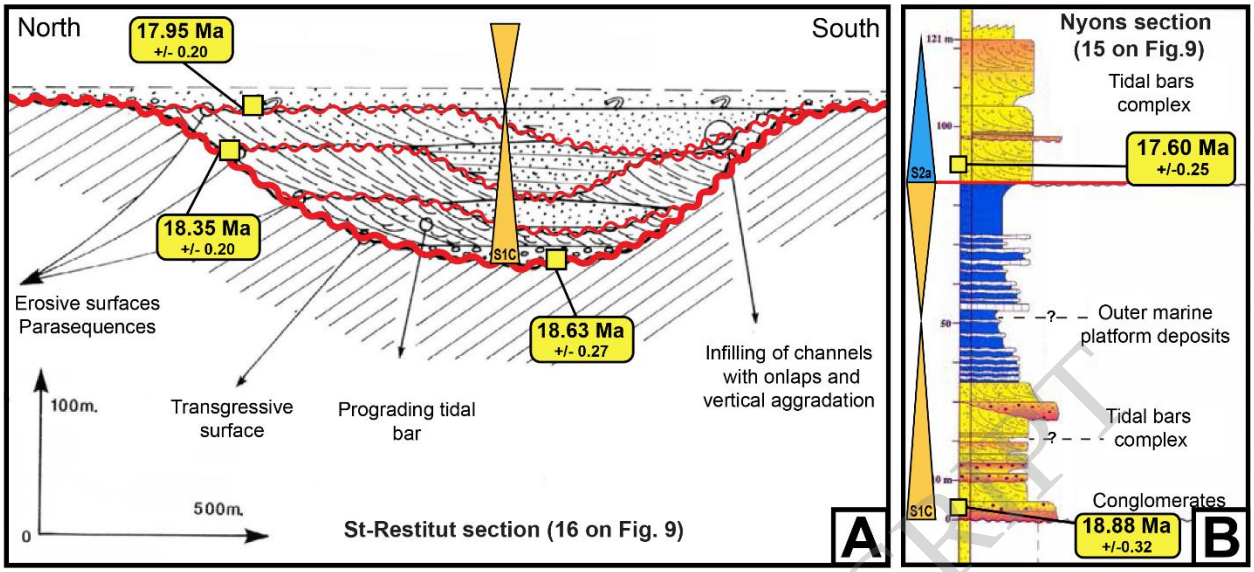

Figure 10

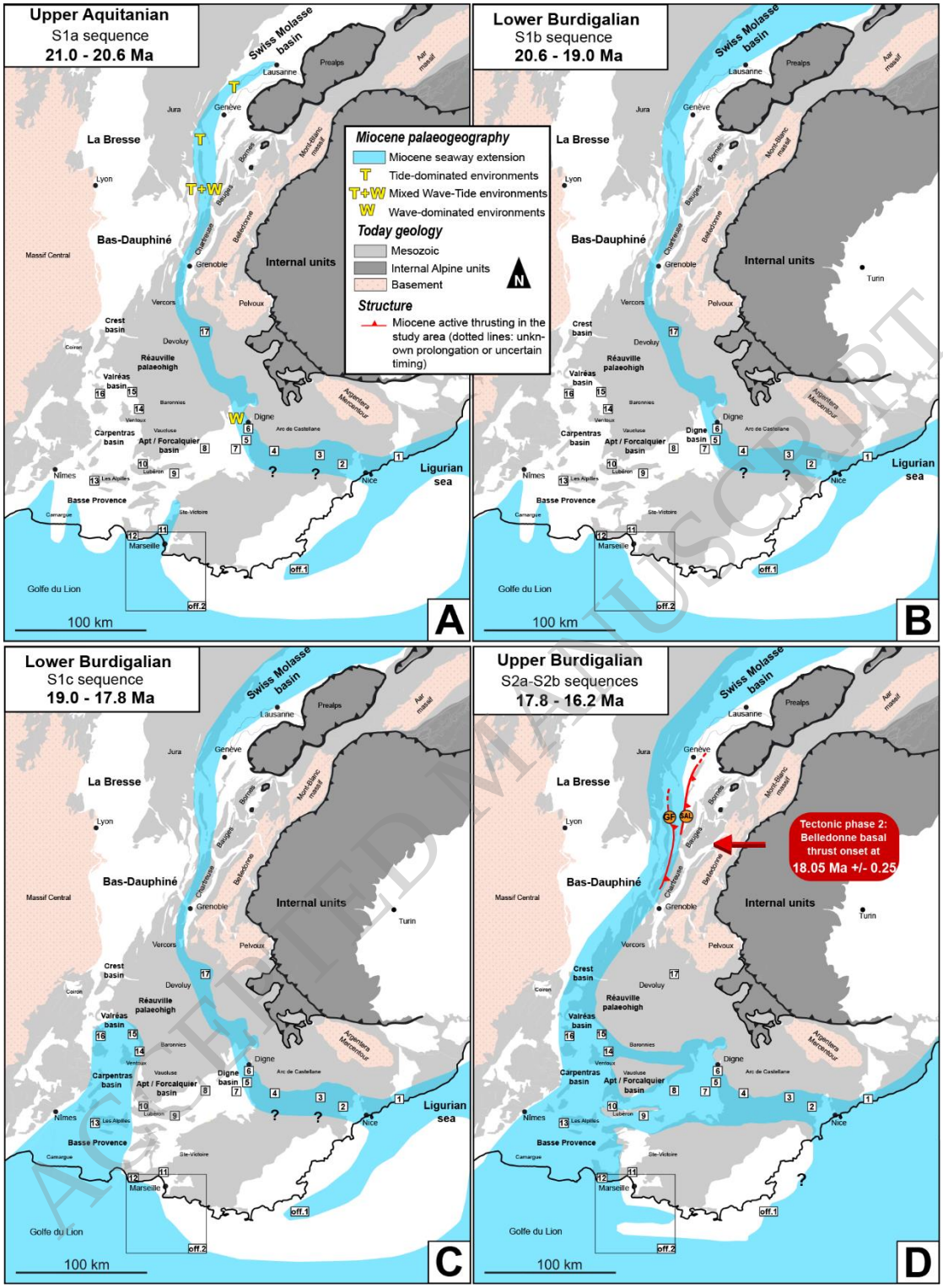

Figure 11

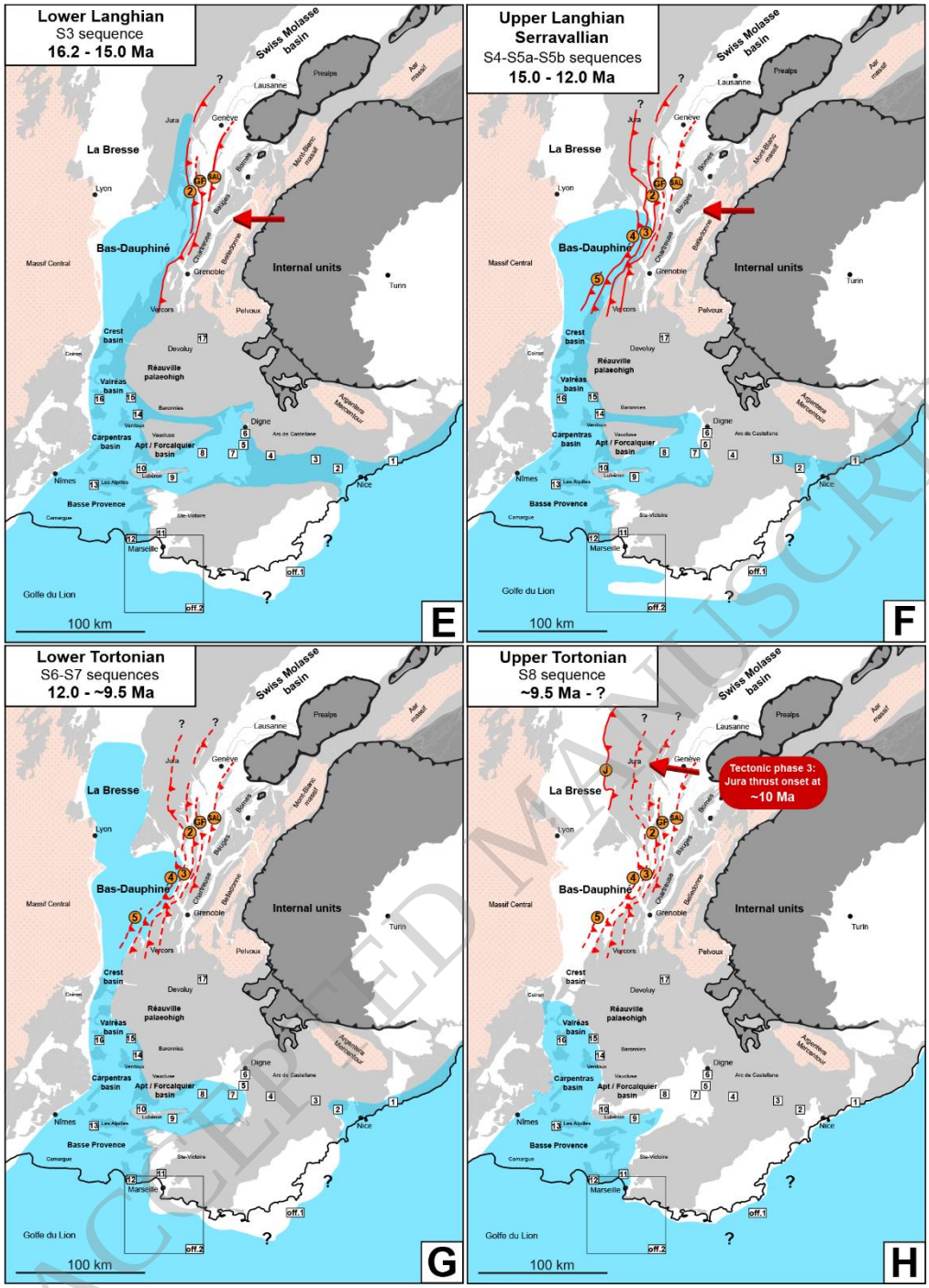

Figure 11(continued)